The impact of sea ice on the air-sea exchange of mercury in the Arctic Ocean

Brian P DiMento[a,*], Robert P Mason[a], Steven Brooks[b], Chris Moore[c]

[a]Department of Marine Sciences, University of Connecticut, 1080 Shennecossett Rd, Groton, CT 06340, USA

[b]Department of Mechanical, Aerospace and Biomedical Engineering, University of Tennessee Space Institute, Tullahoma, TN 37388, USA

[c]Gas Technology Institute, Des Plaines, IL 60013, USA

Abstract

Atmospheric deposition is the main input of mercury (Hg) to the ocean, even in remote locations such as the Arctic. Furthermore, evasion of elemental Hg (Hg^0) is the major sink for oceanic Hg, resulting in air-sea exchange being an important part of the oceanic Hg cycle. To examine the air-sea exchange of Hg in the Arctic Ocean we made high resolution measurements of Hg^0 in surface waters and Hg speciation in the atmosphere during the U.S. Arctic GEOTRACES cruise in 2015 using continuous sampling systems. Additionally, samples were obtained for measurement of Hg and methylmercury (CH_3Hg) in wet deposition and bulk aerosols as well as surface snow and sea ice. We used these measurements from water and the atmosphere to estimate fluxes of Hg^0 from the ocean to the atmosphere (these being potential rates for locations under ice). Overall, concentrations of dissolved Hg^0 (Hg^0_{diss}) were near saturation in ice-free waters (32 ± 30 fM) and resultant fluxes were low, but Hg^0 was highly enriched under contiguous ice (101 ± 98 fM, up to 544 fM) suggesting the continual formation of Hg^0 in waters even when ice covered. Predicted evasion fluxes in these regions, assuming no ice cover, were as high as 492 pmol m^{-2} h^{-1}. Atmospheric Hg^0 concentrations averaged 1.2 ± 0.1 ng m^{-3} with little variation over the course of the cruise, indicating that sea ice acts as a barrier to air-sea exchange in the regions with elevated Hg^0_{diss}. Measurements of Hg in precipitation and aerosols were lower than have been found in more coastal regions of the Arctic. We used these concentrations to estimate deposition of Hg and CH_3Hg to the regions covered by the cruise. Overall, wet deposition represented 88% of the CH_3Hg flux and 38% of the Hg_T flux. Our flux estimates confirm the importance of air-sea exchange in Hg cycling in the Arctic and suggest that evasion was greater than deposition, indicating other sources of Hg to Arctic surface waters. Additionally, our results suggest that fluxes for offshore waters are lower than found by others. From these estimates, we predict how Hg concentrations may respond to future changes in ice cover and other potential impacts of climate change on Hg dynamics and food web bioaccumulation in this important ocean region.

KEYWORDS

Mercury, Elemental mercury, Methylmercury, Gas evasion, Air-sea exchange, Aerosols, Precipitation, Snow, Ice, Arctic

ABBREVIATIONS

Hg^0_{diss}: dissolved elemental mercury; Hg^0_{atmos}: atmospheric elemental mercury; CH_3Hg: methylmercury; Hg_T: total mercury; Hg_R: reactive gaseous mercury; Hg_P/CH_3Hg_P: particulate aerosol mercury/methylmercury; Hg_{oxid}: total oxidized mercury; MIZ: marginal ice zone

HIGHLIGHTS

- Dissolved Hg^0 was supersaturated under ice but near saturation in open waters
- Sea ice acted as a barrier to air sea exchange of Hg
- Atmospheric Hg^0 concentrations (averaging 1.2±0.1 ng m^{-3}) were relatively constant
- Hg in precipitation and aerosols lower over open ocean than in coastal locations
- Hg^0 fluxes were predicted for open and ice-covered waters

1 Introduction

Mercury (Hg), a global contaminant, is of significant interest in the Arctic due to its toxicity and presence in an environment far removed from sources of anthropogenic emissions. Elevated Hg concentrations in Arctic biota are believed to largely be derived from atmospheric deposition (AMAP, 2011), which has increased in remote locations threefold since pre-industrial times (Kirk et al., 2012; Lindberg et al., 2007). A long residence time (6-12 months) in the atmosphere results in the transport of elemental mercury (Hg^0) over long distances from various natural and anthropogenic sources at lower latitudes, including coal combustion and other industrial processes (Corbitt et al., 2011; Slemr et al., 1985). This long-range transport and the remote location of the Arctic make the attribution of sources of Hg to the polar region more difficult.

Ice cover on a large portion of the Arctic Ocean for much of the year impacts air-sea Hg exchange as well as photochemical processes, in addition to creating challenging conditions for sampling the Arctic. The Arctic is uniquely differentiated from other marine ecosystems by its extensive continental shelf (~50% of the Arctic Ocean surface area), and large freshwater inputs from ice melt and river runoff that result in salinity driven stratification of the surface mixed layer. These features, along with its remote location and unique atmospheric events, can affect the fate and distribution of Hg and methylmercury (CH_3Hg) and thus its accumulation and impact on humans who rely on Arctic marine mammals and fish for subsistence (AMAP, 2011). Concerns raised over the health of these indigenous people and the animals they consume from CH_3Hg exposure has resulted in major research initiatives undertaken to help understand the transport, transformation, and biological uptake of Hg and CH_3Hg in the Arctic marine ecosystem.

A warming climate has resulted in dramatic changes to the vast sea-ice environment in the Arctic over the past decades (Macdonald et al., 2005). Temperatures in the Arctic have risen at a rate nearly twice that of the global average (Bekryaev et al., 2010; Bintanja et al., 2011; Screen and Simmonds, 2010), resulting in a 5-10% decrease per decade in annual mean sea ice extent in many regions of the Arctic (Cavalieri and Parkinson, 2012; Parkinson and Cavalieri, 2008). The biogeochemical cycling of Hg is expected to be sensitive to the rapid changes taking place in the region in recent decades (Macdonald et al., 2005; Stern et al., 2012). An increase in Hg^0 evasion would be expected due to both higher temperatures and lower ice cover, with further enhancement by increased net photochemical Hg(II) reduction under greater ultraviolet radiation, a result of increased Arctic ozone depletion (Bais et al., 2011; O'Driscoll et al., 2006).

Air-sea exchange is a critical part of the global Hg cycle. Changes in the Arctic ecosystem, resulting in alterations in Hg inputs, have increasingly driven highly variable CH_3Hg concentrations in upper trophic-level marine biota in recent decades. These changes are greater than would be expected from external anthropogenic emissions alone (Chaulk et al., 2011; Macdonald et al., 2005; Outridge et al., 2008; Stern et al., 2012; Wang et al., 2010). Wet and dry deposition are the dominant sources of Hg to the ocean, accounting for 70% or more of the inputs, while gas evasion is the dominant sink, accounting for about 90% of the outputs (Driscoll et al., 2013; Fitzgerald et al., 2007; Lamborg et al., 2014; Mason et al., 2012). Springtime atmospheric mercury depletion events (AMDE) due to Hg^0 oxidation by bromine (Br) radicals result in the increased deposition of the water soluble divalent Hg(II) species (Ariya et al., 2004; Schroeder et al., 1998; Steffen et al., 2008). Other studies have shown that photochemical

reduction in the surface ocean and snowpack results in the evasion of approximately half of the deposited Hg (Dastoor et al., 2015; Kirk et al., 2006; Lalonde et al., 2002). These events control the magnitude and timing of Hg flux into the aquatic ecosystem, where it can then be transformed to CH_3Hg and accumulated into biota, reemitted as Hg^0, or trapped under the ice.

Recycling of Hg in the surface ocean through redox cycling and air-sea exchange extends the response time of Hg in the surface ocean to changes in anthropogenic inputs. CH_3Hg concentrations are indirectly impacted due to the effects of deposition and evasion on concentrations of total Hg (Hg_T). Elevated CH_3Hg concentrations found in Arctic fish and marine mammals are likely a result of increased deposition as well as enhanced biomagnification resulting from climate-driven shifts in ecosystem characteristics and trophic structure (Braune et al., 2015; Clarkson and Magos, 2006; Mahaffey et al., 2011; Stern et al., 2012). Therefore, in order to accurately predict the response of oceanic Hg_T and CH_3Hg concentrations to changing anthropogenic inputs and a warming climate, we need to develop a comprehensive understanding of the factors affecting Hg^0 gas exchange at the ocean surface.

With the exception of the Arctic Ocean, high resolution measurements of Hg^0_{diss} in surface waters have revealed relatively consistent concentrations within a geographic region (Andersson et al., 2008a; 2008c; Kuss et al., 2011; Mason et al., 2017; Soerensen et al., 2014; 2013). In regions such as the western North Atlantic, Hg inputs were determined to be a potential driver of differences in Hg^0_{diss} concentrations when moving from the continental shelf to offshore waters (Soerensen et al., 2013). In the Arctic, in addition to waters influenced by river discharge, ice-cover regions were also found to have higher [Hg^0_{diss}] (Andersson et al., 2008c). Evasion of this Hg^0 also contributes to elevated concentrations in the atmospheric boundary layer (Soerensen et al., 2010; Strode et al., 2007). While modeling efforts suggest a drastic increase in Hg^0 evasion since the pre-industrial era, flux calculations often rely on short term measurements and thus might not reflect yearly averages (e.g., Mason et al., 1998). More data is therefore required to further constrain such estimates.

Understanding Hg speciation, transformations, and air-sea exchange in Arctic waters is crucial to determining controlling factors in the ultimate bioaccumulation of CH_3Hg in marine food webs. The objective of this study was therefore to improve our knowledge of Hg air-sea exchange in the Arctic through measurements in surface waters as well as the atmospheric boundary layer. Based on limited previous data in the Arctic, we hypothesized that the concentration of Hg^0_{diss} would be positively correlated with sea ice coverage and duration due to the hindrance of evasion. We also predicted that Hg^0 concentrations and evasional fluxes would be lower away from riverine discharges where Hg inputs are less, with biological processes promoting the oxidation of Hg^0 and facilitating its removal by particle settling in waters along the continental shelf. Using measurements of CH_3Hg and Hg_T in precipitation and aerosols, we estimated the Hg inputs from the atmosphere to the surface ocean, and contrasted these with calculated gas evasion fluxes. Finally, we compare our results with measurements made in other regions as well as previous attempts to model Hg cycling within the Arctic.

2 Materials and Methods

Sampling methods

Simultaneous atmospheric Hg^0 and Hg^0_{diss} measurements (five minute temporal resolution) were made aboard the United States Coast Guard Cutter (USCGC) *Healy* on the U.S. Arctic GEOTRACES cruise in the Western Arctic Ocean from August 9, 2015 to October 12, 2015, from Dutch Harbor, Alaska to the North Pole and back. The cruise proceeded northward along the western leg of the track (~180° W) and returned southward along the eastern leg (~150 °W) (Fig. 1). All figures of underway data are plotted with the western leg of the cruise on the left and the eastern return leg of the cruise on the right. The marginal ice zone (MIZ) was found from 73.5-81 °N on the western leg and 79-77.5 °N on the eastern leg, with contiguous ice in between (81-90-79 °N).

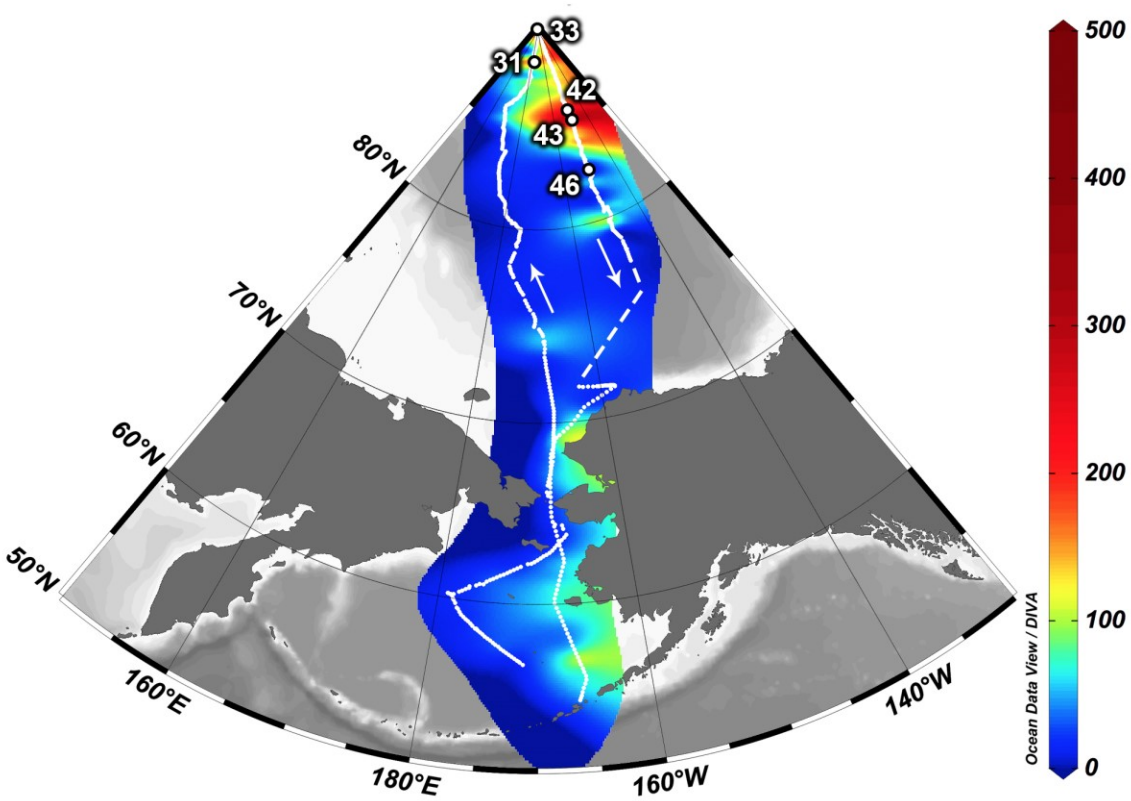

Fig. 1. The U.S. Arctic GEOTRACES cruise track and dissolved Hg^0 (Hg^0_{diss}) concentrations (fM). The cruise track is represented in white, with the dashed line on the southward leg of the cruise representing the section where underway data collection was stopped. The numbered locations are the stations where ice cores were taken. Hg^0_{diss} data interpolation was done using

the Data-Interpolating Variational Analysis (DIVA) software tool in Ocean Data View (Schlitzer, 2015).

Atmospheric Hg measurements in the marine boundary layer were made using the suite of Tekran modules (2537A/1130/1135) for the determination of Hg^0, reactive gaseous Hg (Hg_R), fine particulate Hg (Hg_{PF}), and total oxidized Hg (Hg_{oxid}) using methods described in the literature (Gichuki and Mason, 2014; Landis et al., 2002; Laurier et al., 2003; Lindberg et al., 2001). The inlet to the denuduer has an elutriator attached which removes aerosols < 2.5 μm, which would deposit onto the denuder walls if not removed (Landis et al., 2002). Thus, particulate concentrations determined by the Tekran do not represent the bulk aerosol but only the fine fraction. The sampling inlet was at a height of 9.5 m above sea level. After the initial instrument external calibration, manual injections to check calibration were repeated weekly to check calibration. Internal calibrations were repeated every 47 hours to the system so it was calibrated at different times every other day. The detection limits for these atmospheric measurements were < 0.1 ng m^{-3} Hg^0, 1.1 pg m^{-3} Hg_R and Hg_{PF}, and 3.5 pg m-3 Hg_{oxid}.

Hg^0_{diss} concentrations were determined using a continuous equilibrium system (Andersson et al., 2008a; Mason et al., 2017; Soerensen et al., 2014), which was developed to make high resolution measurements underway using the ship's seawater intake at 7m depth. Briefly, the opposite flow principle was used to establish a continuous equilibrium between the aqueous and gaseous phases by exchanging Hg^0 from the water into counter-flowing air, introduced as bubbles by sparging. The gaseous Hg^0 in the air equilibrated with the water phase was dried prior to entering the Tekran. The measured Hg^0 concentration in the outgoing gas ($[Hg^0_{gas}]$) is equivalent to the Hg^0_{diss} concentration multiplied by the dimensionless Henry's Law constant ($k_{H'}$) at the current temperature and salinity of the water.

$$[Hg^0_{diss}] = [Hg^0_{gas}] / k_{H'} \quad (1)$$

This method can measure both Hg^0_{diss} and dimethylmercury ($(CH_3)_2Hg$), but measurements of $(CH_3)_2Hg$) made aboard the ship (K. Bowman, personal commun.) indicate that it represented only a small fraction (<5%) of the total dissolved gaseous Hg in the surface waters. Therefore, the measurements were assumed to reflect the concentrations of Hg^0_{diss}.

The same intake used for the Hg^0_{diss} measurements was also used to continuously (every 15 seconds) determine surface temperature, salinity, and fluorescence. Along with wind speed and Hg_{eq} measurements, these data were averaged into hourly values before calculating Hg^0_{diss} concentrations and gas exchange parameters. Due to concerns of contamination when the ship was stationary, data collected while the ship was on station were removed from the underway Hg^0_{diss} measurements plotted in the figures. As was the case on the previous GEOTRACES cruises, these data were not used in the flux calculations (Mason et al., 2017). Generally, the Hg^0_{diss} concentrations while the ship was on station were higher than while underway.

An automated N-CON rain sampler (designated for Hg analysis) was used to collect rain (falling snow was not collected for Hg analysis) during the cruise. It was arranged and operated to avoid contamination from the ship and sea spray. Low rainfall warranted ultra high purity water rinses of the collection funnel in all but one sample, with the rinse and sample combined and recovered for analysis. Two deployment blanks were also collected.

Fourteen bulk aerosol deployments were made over periods of three to five days using high-volume aerosol samplers following methods in Morton et al. (2013). During each deployment, aerosol samples were collected in triplicate on pre-combusted glass-fiber (GFF) or quartz fiber (QMA) filters. Unused filters were set aside for blank analysis. Sampling duration lasted an average of 31.0 h (11.0 to 80.0 h) with an average volume filtered of 172.5 m^3 (60.6 to 451.9 m^3).

Ice cores were sampled using a trace metal clean corer at five stations, with duplicate cores collected at two of the five locations. Ice stations were located between 88.4 °N on the northward leg and 82.5 °N on the southward leg of the cruise. Whole ice cores, collected with a trace metal clean corer, were returned to the Hg clean facility where colleagues on the ship subsampled them into sections. Once the cores were divided, the subsections were placed in Teflon collection containers and defrosted under laminar flow conditions. The samples were then decanted into Teflon bottles and refrozen. The collection containers were cleaned and re-used for the next ice core. Cores did not extend to the bottom of the ice because of the concern that the samples would not be representative of the ice itself due to infiltration of seawater during coring. Porous ice also potentially resulted in the loss of brine waters within the core during coring.

Triplicate bulk snow samples were collected at the same sites as the ice cores. Snow was collected using an acid cleaned HDPE shovel, and transported in a LDPE container before being melted and subsampled on board.

After collection, snow and ice samples were melted and transferred to acid-cleaned glass bottles (I-CHEM Certified 200 series), and precipitation samples were stored in Teflon FEP bottles. Aerosol filters were stored in acid cleaned polystyrene petri dishes. All samples were kept frozen at -20 °C in the dark, and were transported back to the University of Connecticut for analysis.

Analytical methods

Methylmercury concentrations were determined following the ascorbic acid-assisted direct ethylation method (Munson et al., 2014) using a Tekran 2700 instrument and autosampler to automate the purging, trapping, and detection via cold vapor atomic fluorescence spectroscopy (CVAFS). Samples were thawed then acidified to 1% (v/v) H_2SO_4 and left to digest overnight before neutralizing with 8N potassium hydroxide (KOH), buffering with 4M acetate, adding 2.5% (w/v) ascorbic acid and finally 1% (w/v) sodium tetraethyl borate (NaTEB) to ethylate the CH_3Hg. Sample concentrations were corrected for matrix spike recoveries, which averaged 82 % with a typical relative standard deviation (RSD) of 10 %. Average method detection limits (MDL) were less than 10 fM.

Total mercury concentrations were determined by dual gold-amalgamation CVAFS utilizing a Tekran 2600 instrument in accordance with U.S. EPA Method 1631 (Lamborg et al., 2012; U.S. Environmental Protection Agency, 2002). Briefly, waters were digested with bromine monochloride (BrCl) followed by a pre-reduction step with hydroxylamine hydrochloride ($NH_2OH \cdot HCl$). Inorganic Hg(II) was then reduced to Hg^0 using stannous chloride ($SnCl_2$) prior to automated analysis on the Tekran. Matrix spike recoveries averaged 98 ± 9 %, and the MDL was 0.25 pM.

Aerosol filters were digested in acid-cleaned 15-mL centrifuge tubes with 10 mL of 4.57 M trace metal grade HNO_3, placed in a covered 60 °C water bath for 12 hours (Hammerschmidt and Fitzgerald, 2006; 2005). A subsample of this digest was taken for CH_3Hg analysis, and the remainder was further digested with BrCl overnight at room temperature. Method detection limits were about 0.1 pg m^{-3} for Hg_T and 2 fg m^{-3} for CH_3Hg, based on the average volume of air filtered and the volume of digest analyzed.

Hg^0 concentration and flux calculations

Flux calculations were performed following the approach of Soerensen et al. (2010) and Mason et al. (2017). The flux (F, pmol m^{-2} d^{-1}) is defined as follows:

$$F = k_w([Hg^0_{diss}]-[Hg^0_{atmos}]/ k_{H'}) \quad (2)$$

where k_w (m hr^{-1}) is the water side mass transfer coefficient (gas-transfer velocity), $[Hg^0_{diss}]$ (ng m^{-3}) is the concentration of Hg^0 in water, and $[Hg^0_{atmos}]$ (ng m^{-3}) is the concentration of Hg^0 in air. The mass transfer coefficient (k_w) is calculated from the wind speed and Schmidt number for Hg and CO_2, which is equal to the ratio between the kinematic viscosity of the water and the aqueous diffusivity of Hg (Andersson et al., 2008b). Positive fluxes represent evasion out of the ocean to the atmosphere, while negative fluxes are into the ocean. The degree of saturation (S) is defined as:

$$S = [Hg^0_{diss}]/[Hg^0_{diss}]_{eq}*100 \text{ where } [Hg^0_{diss}]_{eq} = [Hg^0_{atmos}]/ k_{H'} \quad (3)$$

where $[Hg^0_{diss}]_{eq}$ represents the concentration of Hg^0 in equilibrium with the air.

Wet and dry deposition were estimated using the concentration of Hg in precipitation and aerosols, along with the Hg_R concentration, using the parameters summarized in Soerensen et al. (2016). Wet deposition is calculated by the Hg concentration multiplied by the annual rain/snow fall, while the dry particulate deposition flux is equal to the product of the measured aerosol and Hg_R concentrations and the dry deposition velocity (Mason et al., 2017). Because Hg_R values are expected to show significant seasonal variation because of substantial Hg_R formation during Hg depletion events in the spring (Lindberg et al., 2001), flux values were calculated on a per month basis.

3 Results

Trends in dissolved Hg

Trends in Hg^0_{diss} concentration in the Arctic Ocean (Fig. 2) will be discussed in terms of three geographical regions – contiguous ice (81 – 90 – 79 °N), the MIZ (73.5 – 81 °N, 79 – 77.5 °N), and open water (south of the MIZ). The overall average hourly concentration of Hg^0_{diss} was 68 ± 83 fM, ranging from 3.9 to 454 fM. In open water, the average concentration was 32 ± 30 fM, while under contiguous ice the average was significantly higher ($p < 0.0001$), 101 ± 98 fM, reaching a maximum instantaneous value of 544 fM under the contiguous ice. Concentrations were elevated near shore on the return leg of the cruise suggesting increased coastal inputs from a change in water circulation during the duration of the cruise.

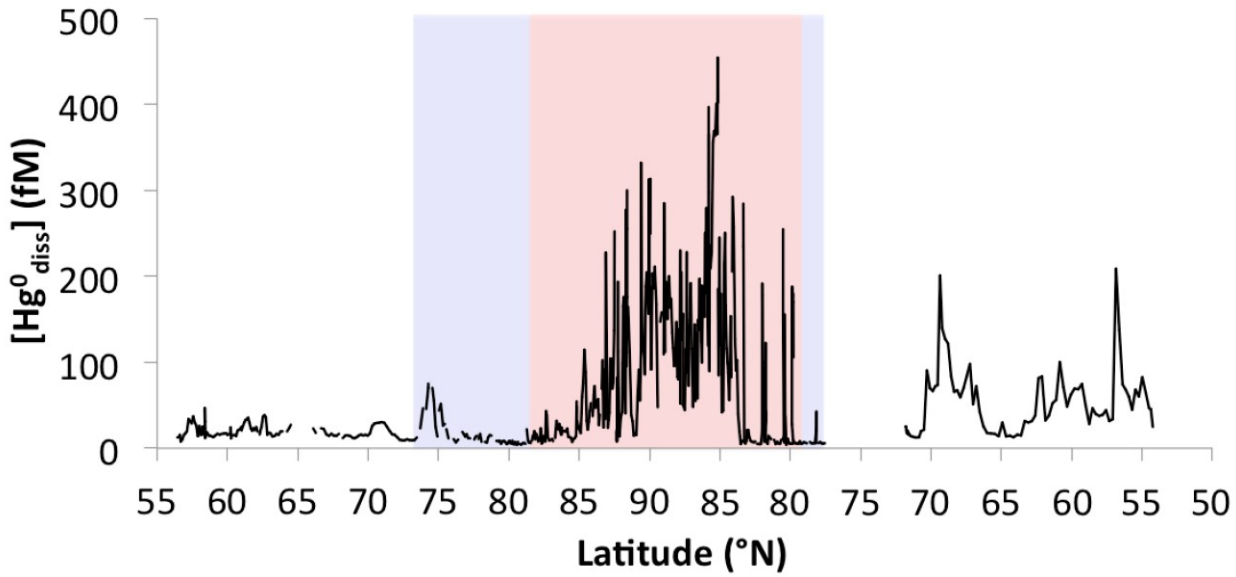

Fig. 2. Dissolved Hg^0 (Hg^0_{diss}) along the U.S. Arctic GEOTRACES cruise track during the marginal ice (light blue shading; 73.5-81°N, 79-77.5°N) and contiguous ice (light red shading; 81-90-79°N) zones.

Trends in atmospheric Hg

Variability in atmospheric Hg^0 concentrations in the marine boundary layer is much lower than sea surface Hg^0_{diss}. Average hourly concentrations (Fig. 3) ranged from 0.86 to 1.88 ng m^{-3}, with an average of 1.2 ± 0.1 ng m^{-3} (Table 1). The highest concentrations were observed in the Bering Sea and Bering Strait. Following a brief decline in Hg^0 around 75 °N concentrations briefly rose in the MIZ before slowly returning to average values over the continuous ice zone.

Concentrations of Hg_R and Hg_{PF} measured by the Tekran speciation units were very low, averaging 1.7 pg m^{-3} and 2.2 pg m^{-3}, and were therefore within a factor of two of the detection limits for each species. Particulate bulk aerosol CH_3Hg (CH_3Hg_{PB}) and total Hg (Hg_{PB}) concentrations (Fig. S3) measured on filters were generally low, with many measurements below the detection limit of the instrument. Average CH_3Hg_{PB} concentrations were 1.4 ± 1.9 fg m^{-3}, while Hg_{PB} averaged 0.33 ± 0.34 pg m^{-3} (Table 1). The similarity between the values of Hg_{PF} and Hg_{PB} indicates that most of the Hg was in the fine fraction of the aerosol phase and not associated with larger particles, which would predominantly be sea salt in the Arctic. The percent CH_3Hg in the aerosol was 0.5 ± 0.5%, lower than was found in precipitation.

The concentration of Hg_{oxid} measured by the total pyrolyzer averaged 6.9 pg m^{-3}. This value should be equivalent to Hg_R + Hg_{PB}, and again, given the low values found on the cruise, the values are comparable. The low values for both the aerosol and the Hg_R are an indication that dry deposition is not an important atmospheric sink of Hg in this region during the time of the cruise.

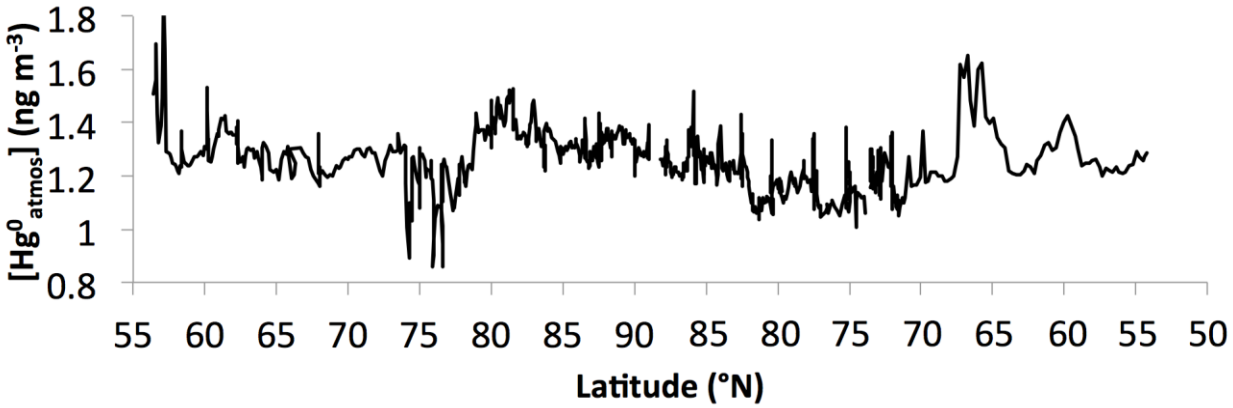

Fig. 3. Underway atmospheric Hg concentrations ([Hg^0_{atmos}]) during the U.S. Arctic GEOTRACES cruise.

Hg in precipitation

Rain collected during this cruise had an average CH_3Hg concentration of 0.033 ± 0.028 pM and a Hg_T concentration of 3.1 ± 2.1 pM, with a % CH_3Hg of 1.2 ± 0.6 % (Table 1). Most rain events were small with minimal or trace amounts of precipitation collected. Concentrations were variable with no observed strong geographic trends for both rain and aerosols (Fig. S3, S4).

Table 1

Summary of average methyl (CH_3Hg) and total Hg (Hg_T) concentrations, in addition to percent CH_3Hg, in atmospheric bulk aerosols and precipitation samples, as well as ice cores, snow and melt pond water on the surface of sea ice.

	[CH_3Hg]	[Hg_T]	%CH_3Hg
Bulk Aerosols	1.4 ± 1.9 fg m^{-3}	0.33 ± 0.34 pg m^{-3}	0.53 ± 0.50 %
Precipitation	33 ± 28 fM	3.1 ± 2.1 pM	1.2 ± 0.64 %
Snow	11 ± 1 fM	3.6 ± 1.3 pM	0.41 ± 0.49 %
Melt Pond	97 ± 75 fM	11 ± 9 pM	1.3 ± 0.8 %
Ice Cores	86 ± 120 fM	2.8 ± 2.0 pM	3.5 ± 4.3 %

Ice cores, surface snow and melt ponds

CH_3Hg and Hg_T profiles from ice cores at the five stations sampled are shown in Fig. 4. Higher concentrations were generally found at the surface, decreasing with depth in the core. Percent CH_3Hg was highly variable, averaging 3.5 ± 4.3 % (Table 1), with peak values often observed at the base of the core. No latitudinal trend was observed in concentration or % CH_3Hg.

Falling snow was not collected for Hg analysis during this cruise, but surface snow on ice sheets was collected at ice stations. Average concentrations in snow (Table 1) were 11 ± 1 fM CH_3Hg and 3.6 ± 1.3 pM Hg_T. In melt pond waters, CH_3Hg averaged 97 ± 75 fM CH_3Hg and 11 ± 9 pM Hg_T.

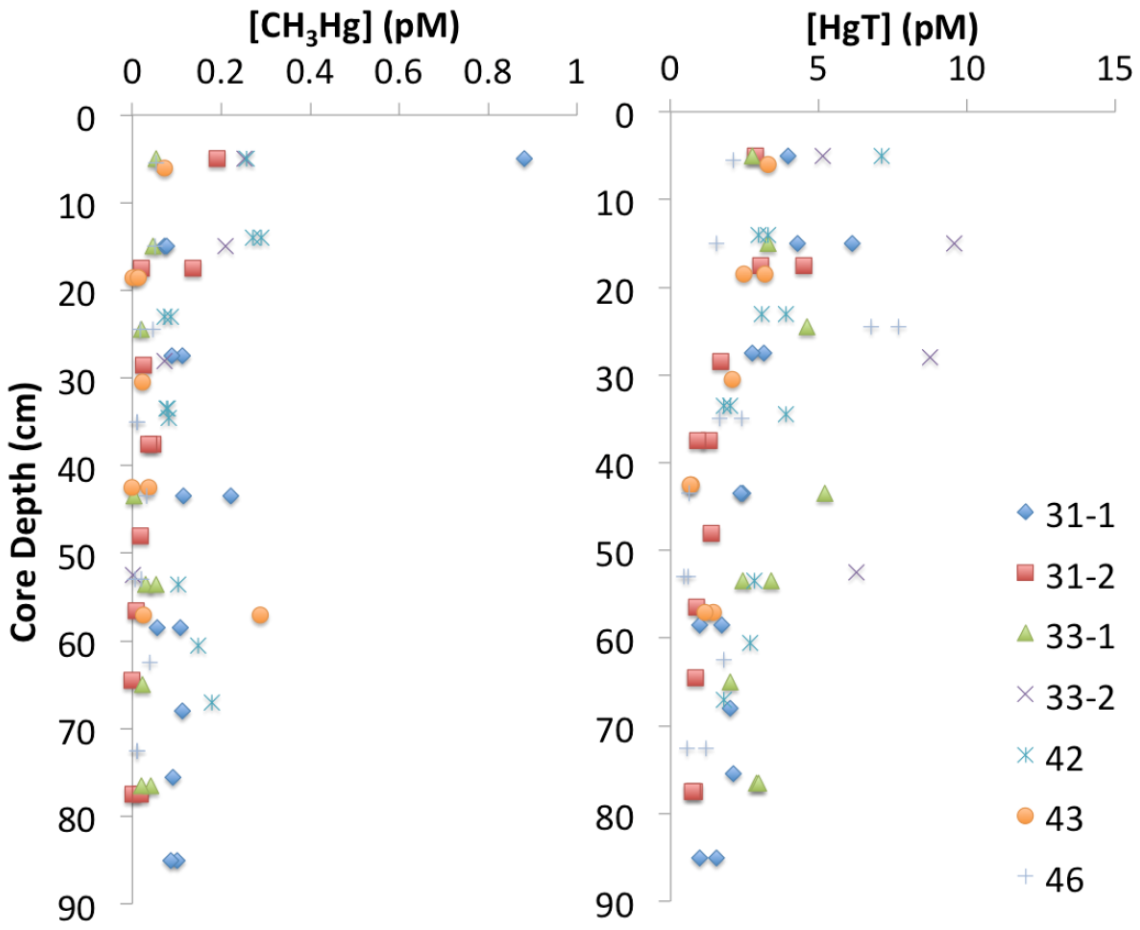

Fig. 4. Methyl (CH_3Hg) and total Hg (Hg_T) concentrations in ice cores taken during the U.S. Arctic GEOTRACES cruise.

4 Discussion

Trends in Hg^0_{diss}

Trends in Hg^0_{diss} concentrations indicate that ice cover acts as a barrier to Hg evasion. Concentrations measured in open water during the early part of the cruise (19 ± 7 fM) are comparable to earlier studies in the region (Andersson et al., 2008c; Kim et al., 2016). Higher concentrations (74 ± 18 fM) were measured by Kim et al. (2016) further south in the Bering Sea, while Andersson et al. (2008c) measured higher concentrations to the north off the coast of Alaska and Russia, possibly because of the earlier timing of the cruise following ice-out. Early in the cruise there was some evidence for a diurnal change in Hg^0_{diss} concentrations (Fig. S7), but this trend was not found later in the cruise. Potential correlations between Hg^0 concentrations and other variables during the early part of the cruise are discussed in the SI (Fig. S8).

Entering the MIZ the concentration did not immediately begin to rise, indicating a lag between ice cover and accumulated Hg^0_{diss} levels (Fig. 2). Peak concentrations measured under the ice were not as high as those measured by Andersson et al. (2008c), although hourly averages mask some of the brief peaks in concentration observed under the ice. The maximum

concentration was observed south of the pole along the eastern return leg of the cruise, 17 times higher than observed on average in the open water, in a location that corresponded with a greater concentration of multi-year ice (NOAA Climate.gov, 2016) (Fig. 5).

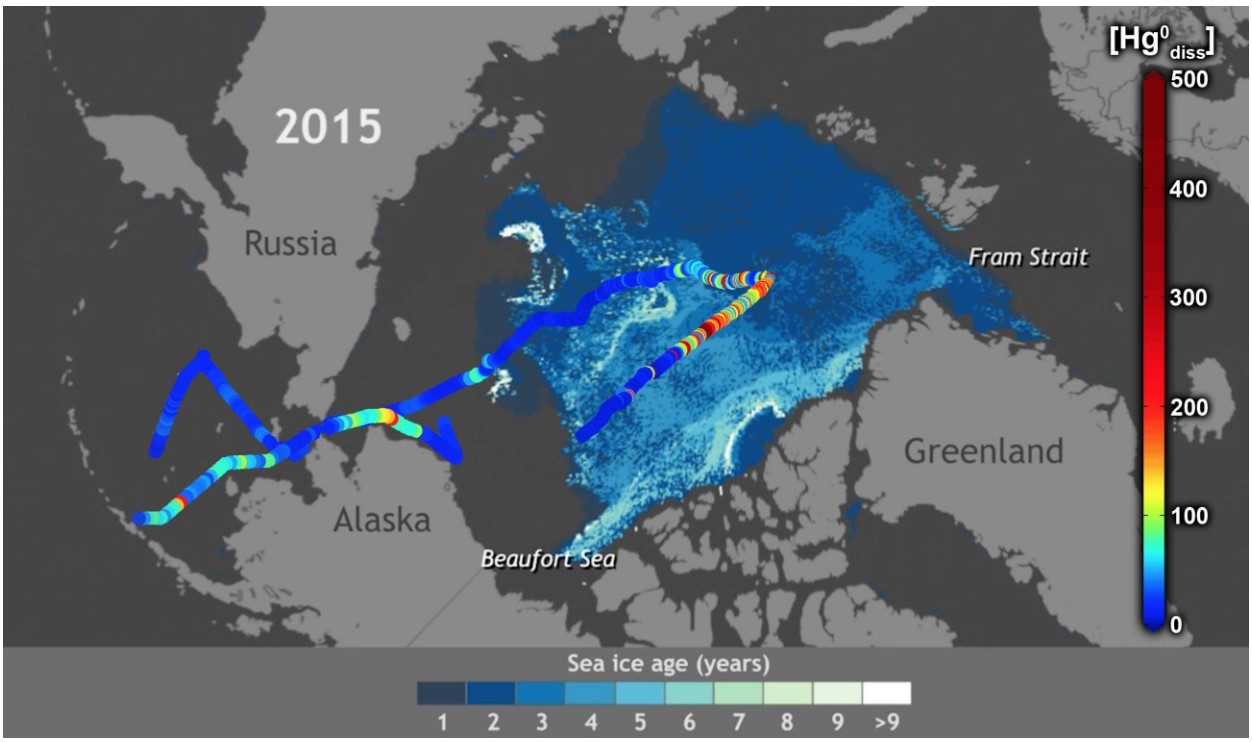

Fig. 5. The dissolved Hg^0 concentrations (fM) along the U.S. Arctic GEOTRACES cruise track overlaid on ice coverage in the Arctic during September, 2015 (NOAA Climate.gov 2016, based on data from Tschudi et al., 2016).

Variability in Hg^0_{diss} concentrations was high under the ice, possibly due to varying extent and duration of ice cover. The presence or absence of leads and open water, both prior to and at the time of sampling, could have contributed to this variability. As shown in Fig. , peaks in Hg^0_{diss} generally occur in regions with near-complete ice cover, indicating the potential for degassing and thus lower concentrations in open leads.

Additional variability in underway data could be due to the movement of the ship, breaking through the ice and mixing the surface water as it finds its way and creates openings in the ice. However, a study of ^{222}Rn concentrations concluded, based on measurements collected from the ship on station and from locations removed from the ship's influence (sampled through ice), that there was no impact of the ship on the ^{222}Rn concentration and profile within the surface mixed layer (Rutgers van der Loeff et al., 2014). Also, at stations under ice, the ^{222}Rn concentrations were close to secular equilibrium suggesting that gas exchange had not occurred to any substantial degree over the timescale needed to reach secular equilibrium (several weeks). While no ^{222}Rn measurements were made while the ship was underway, the results do overall suggest that the large variations found in the Hg^0_{diss} cannot be attributed solely to the ship's movement, ice breaking and associated mixing.

Additionally, the ^{222}Rn data (Rutgers van der Loeff et al., 2014) also suggest limited gas exchange in regions with ice cover, which is consistent with the conclusions of Loose et al. (2011) but contrary to the conclusions of others (e.g. Fanning and Torres, 1991). There is an ongoing debate on the potential for gas exchange in ice-covered regions with leads and other breaks in the ice. The Rutgers van der Loeff et al. (2014) data suggest that the rate of gas exchange in regions with partial ice cover were less than would be predicted based on estimations assuming gas exchange was happening normally in open waters between ice. This is contrary to lab experiments that indicated that gas exchange was enhanced over prediction in partial ice covered waters (Loose et al., 2009). We found no evidence for enhanced gas exchange (i.e. Hg^0_{diss} depletion) at the ice edge stations. The variability under the ice and the inverse relationship between concentration and ice cover do suggest that there could be loss of Hg^0_{diss} from the open waters within the ice. However, as there is no definitive answer in the literature, we have made gas exchange calculations assuming that there is little gas exchange in regions that are dominantly ice covered.

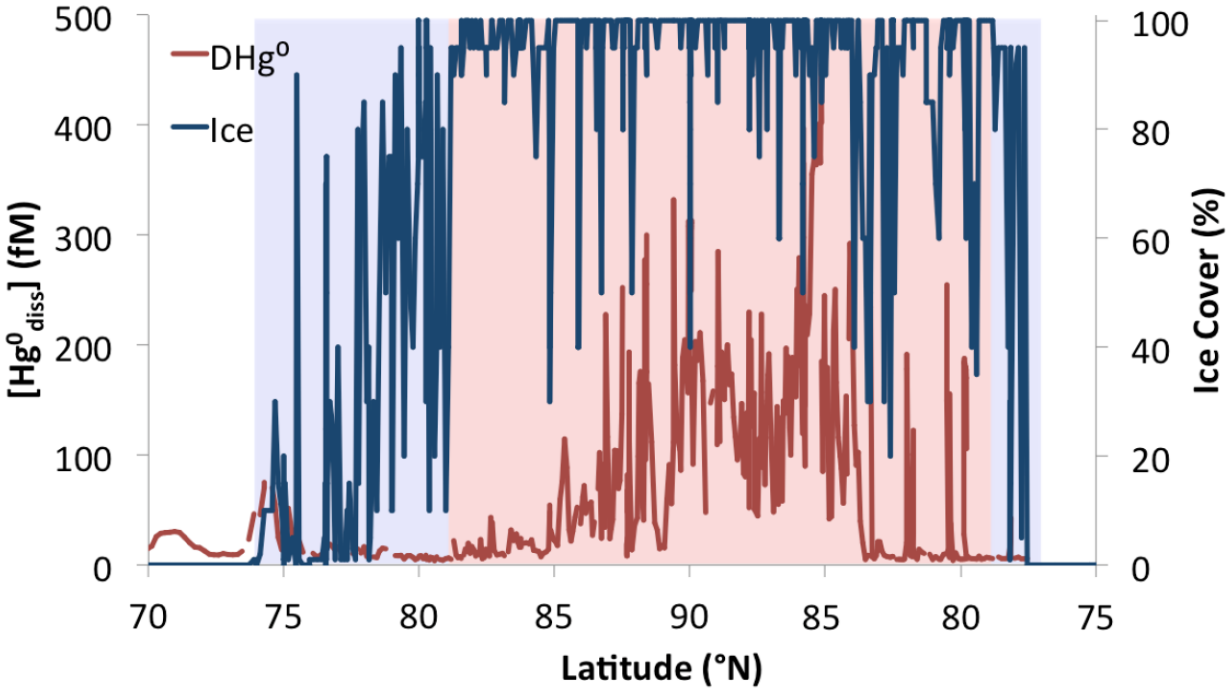

Fig. 6. The dissolved Hg^0 (Hg^0_{diss}) concentration along the U.S. Arctic GEOTRACES cruise track during the marginal ice (light blue shading; 73.5-81°N, 79-77.5°N) and contiguous ice (light red shading; 81-90-79°N) zones.

Hg^0 air-sea exchange

After using the atmospheric Hg^0 concentrations and calculated $k_{H'}$ values to calculate an equilibrium Hg^0_{diss} concentration, we determined the percent saturation of Hg^0 (Equation 3) in the surface waters of the Arctic (Fig. S6, Table 1). In the absence of contiguous sea ice, Hg^0_{diss} concentrations were typically near saturation. On the western leg of the cruise in open water (south of 73.5 °N) the percent saturation was 61 ± 25 %, while on the eastern return leg it was

145 ± 116 %. The overall average percent saturation for open water was 97 ± 88 %. Increased saturation on the eastern leg was a result of elevated Hg^0_{diss} concentrations near shore. In the MIZ, where Hg^0_{diss} concentrations had not had a chance to build (or rather had already evaded), the percent saturation was 39 ± 46 %. Concentrations were strongly supersaturated under contiguous ice, increasing to an average of 230 ± 228 % with a maximum of 1105 %. The maximum degree of saturation observed by Andersson et al. (2008) in this region was 1800%. Undersaturation has sometimes been observed in other waters such as the South China Sea, where decreased production of Hg^0_{diss} was attributed to low temperatures in the winter (Tseng et al., 2013). For many warmer regions of the ocean, such as the North Atlantic and Southeastern tropical Pacific, supersaturation has been observed, but not to the same extent that we calculated under the ice (e.g., Mason et al., 2017).

Estimated Hg^0 evasion in the Arctic was largely minimal in open offshore waters (Fig.7). Toward the North Pole, there was the potential for higher Hg^0 evasion due to the elevated levels of Hg^0_{diss}; however, the sea ice acts as a barrier and prevents this flux from the ocean. A hypothetical flux was calculated regardless, using below ice water temperatures as well as local wind speed and atmospheric Hg^0 concentrations. Open water Hg^0 fluxes averaged 2 ± 14 pmol m^{-2} h^{-1}, with an average of -2 ± 2 pmol m^{-2} h^{-1} on the western leg and 8 ± 19 pmol m^{-2} h^{-1} on the eastern return leg pmol m^{-2} h^{-1} of the cruise. In the MIZ, average fluxes were 3 ± 5 pmol m^{-2} h^{-1}, increasing to a potential flux (if the ice was removed) of 14 ± 52 pmol m^{-2} h^{-1} (Table 1) under contiguous ice. Maximum predicted evasion values reached 492 pmol m^{-2} h^{-1}, which was very similar to the maximum evasion rate observed by Andersson et al. (2008) along the Alaskan coast (490 pmol m^{-2} h^{-1}). Fluxes in open water were similar in magnitude to values estimated in other regions across the globe, from the Pacific and Atlantic Oceans to coastal waters (Andersson et al., 2007b; Ci et al., 2016; Kuss et al., 2011; Mason et al., 1999; Soerensen et al., 2014).

As has been observed previously, both variations in Hg^0_{diss} and wind speed drive the evasion of Hg^0 (Kuss et al., 2011; Soerensen et al., 2014; 2013). However, because of the substantial differences between concentrations in ice-free and covered waters there were no general observable trends between the Hg^0_{diss} concentrations and fluxes and other ancillary variables (Fig. S2). In addition to the elevated flux indices during periods of elevated Hg^0_{diss} levels, peaks in fluxes were also calculated at times of increased wind speed events (Fig. S1), resulting in the spikes in fluxes observed in Fig.7. Elevated evasion on the eastern leg of the cruise is a result of higher Hg^0_{diss} concentrations as well as increased winds.

Despite increased Hg^0_{diss} concentrations and percent saturation values over 100% at high latitudes, no significant increase in Hg^0_{atmos} was observed, confirming that sea ice acts as an effective barrier for the transport of volatile Hg^0. Average Hg^0_{atmos} concentrations (1.2-1.3 ng m^{-3}; Table 2) were also generally lower than have been measured in coastal Arctic sites such as Alert, Canada (e.g., Kirk et al., 2012).

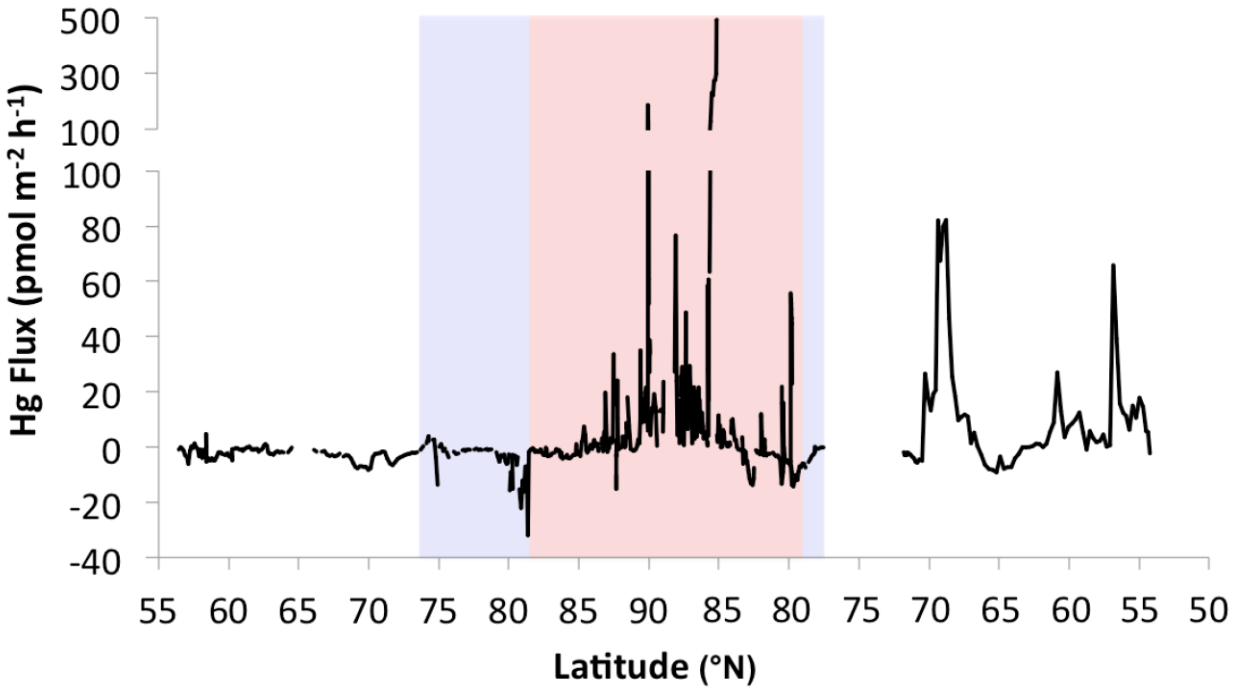

Fig. 7. Evasion of dissolved Hg^0 out of the surface ocean along the U.S. Arctic GEOTRACES cruise track. Values under ice cover (marginal ice: light blue, 73.5-81°N, 79-77.5°N; contiguous ice: light red 81-90-79°N) are theoretical fluxes.

Accumulation of Hg^0_{diss} under sea ice has obvious ramifications for Hg cycling given the future predicted changes in the timing and extent of annual ice coverage. Using the average surface concentration under the ice of 101 fM and a calculated average equilibrium concentration of 32 fM for the same region, along with an average K_w of 0.177 m hr^{-1} based on measured wind speeds, we calculated the time to equilibrium after the theoretical sudden removal of sea ice from the contiguous ice zone. Flux rates were calculated hourly as surface concentrations dropped until equilibrium was reached. After 15.5 days the concentration was within 5% of the equilibrium value, and after 23 days it was within 1%. This timing makes sense based on previously observed peaks in atmospheric Hg^0 concentrations due to evasion from the surface ocean, which occur later than peaks due to revolatilization of Hg from snowmelt (Dastoor and Durnford, 2014). The calculation serves as a rough estimate, as other processes (e.g., deposition and photochemical cycling) will resume upon the removal of ice. The formation of sea ice acts as a physical barrier to gas exchange, allowing Hg^0_{diss} concentrations to build in surface waters. Although a small portion of the UV radiation makes it through the ice (Perovich, 2006), net biological Hg(II) reduction is likely the primary pathway for Hg(II) reduction in the Arctic compared to other oceans where photochemical reduction dominates (Kirk et al., 2012; Poulain et al., 2007; Soerensen et al., 2010). Similar time scales to those predicted for evasion are expected for accumulation of Hg^0_{diss} under contiguous ice. This prediction is backed up by our observation of low Hg^0_{diss} concentrations in MIZs where water masses have likely not been trapped under mobile ice sheets for very long.

Table 1

Summary of average Hg^0 concentrations in water ($[Hg^0_{diss}]$) and air ($[Hg^0_{atmos}]$) and average Hg^0 air-sea flux values in open water, the marginal ice zone (MIZ), and under contiguous ice. *Flux values under ice are theoretical based on ice-free conditions.

	Open Water	MIZ	Contiguous Ice
$[Hg^0_{diss}]$ (fM)	32 ± 30	16 ± 17	101 ± 98
$[Hg^0_{atmos}]$ (ng m^{-3})	1.2 ± 0.1	1.2 ± 0.1	1.3 ± 0.1
% Saturation	97 ± 88	39 ± 46	230 ± 228
Hg Flux (pmol m^{-2} h^{-1})	2 ± 14	-3 ± 5	14 ± 52*

Precipitation and aerosols

Precipitation CH_3Hg and Hg_T concentrations were similar to those found in surface snow. Hg_T concentrations were lower than typically reported in lower regions of the Arctic. For example, annual mean concentrations of 25-46 pM were reported in the Canadian sub-Arctic (Sanei et al., 2010). Lower concentrations have been measured in open ocean regions of the central Pacific, averaging 11 ± 6 pM (Mason et al., 2017). CH_3Hg measurements in precipitation are more limited. While $\%CH_3Hg$ values were comparable to those found in other remote ocean locations, CH_3Hg concentrations in the North Atlantic averaged 0.41 ± 0.23 pM (Mason et al., 2017). Other studies in the Canadian Arctic Archipelago also found higher CH_3Hg concentrations averaging 0.13 to 0.50 pM (Hammerschmidt et al., 2006; Lehnherr et al., 2012).

In agreement with previous research (Cobbett et al., 2007; Kirk et al., 2006; Steffen et al., 2014), Hg_P concentrations measured on aerosol filters (0.33 ± 0.34 pg m^{-3}) were low during the time of the cruise (following the spring AMDE). Cobbet et al. (2007) observed a peak in Hg_P concentrations in Alert, Canada during the transition between the polar night and polar day (February – March) as high as 693.9 pg m^{-3}, but concentrations dropped after this period. Minimum concentrations under 1 pg m^{-3} were reported in multiple studies for other periods of the year, including the time covered by this cruise (Cobbett et al., 2007; Steffen et al., 2014). Average concentrations were generally higher than measured during this study, possibly indicating a decreasing geographic trend away from land moving towards the Pole.

The highest aerosol concentrations corresponded with the deployment that covered the region where there was a spike in Hg^0_{diss} and drop in the concentration of Hg^0_{atmos} at 75 °N, possibly indicating the scavenging of Hg^0_{atmos} (due to oxidation to Hg_R) and deposition into the ocean. Holmes et al. (2009) suggested that any Hg_R produced in the marine boundary layer would be taken up by sea salt particles and rapidly removed from the atmosphere. However, our results do not clearly support such a mechanism, as there is no indication that the aerosol Hg is concentrated onto larger particulates.

Comparing Hg data to measurements of aluminum (Al; C. Buck, personal comm.), a crustal element that has little anthropogenic inputs to aerosols, we conclude that the particulate Hg is not of crustal origin. The Hg/Al (g/g) ratios (Fig. S5) are well above the crustal ratio of ~7 x 10^{-8} (Mason et al., 2017). The lowest ratios were found near the pole with the highest values closer to shore, indicating a larger influence of anthropogenic Hg near the continent.

Ice cores, surface snow and melt ponds

Hg concentrations in ice cores were generally low with higher concentrations at the surface, possibly due to scavenging of Hg_P and Hg_R and the resulting atmospheric deposition, likely following spring AMDEs (Fisher et al., 2013; Steffen et al., 2014). Concentrations deeper in the core were lower, matching values found in surface waters under the ice (0.1 ± 0.1 pM CH_3Hg, 1.4 ± 0.4 pM Hg_T; Bowman, personal comm.). Because samples were unfiltered, higher values of %CH_3Hg found could indicate either patches of biogenic particles (algae), or possibly regions of methylation in the ice (Gionfriddo et al., 2016). Average Hg_T and CH_3Hg concentrations (2.8 and 0.09 pM, respectively; Table 1) were very similar to other studies in the Arctic and Antarctic (Beattie et al., 2014; Chaulk et al., 2011; Cossa et al., 2011).

Chaulk et al. (2011) found low and consistent concentrations in first year ice in the Southern Beaufort Sea of the Arctic, measuring concentrations ~2.5 pM in most of the ice core, with higher values up to 15 pM at the ice-snow interface. In multi-year ice, concentrations above 20 pM were found at the surface. The Hg_T concentrations decreased sharply with depth, but unique to the multi-year ice were cyclic features with several peaks rising to ~8 pM. Similar to our study, concentrations deeper in the core were comparable to the underlying water, but concentrations in the surface ice as not as elevated as previously reported. Again, in the Beaufort Sea and McClure Strait, Beattie et al. (2014) measured Hg_T and CH_3Hg concentrations in multi-year ice. Trends with depth were similar, but concentrations rose moving from the Beaufort Sea into the McClure Strait, with Hg_T concentrations as high as 60.8 pM were found in surface ice at the McClure Strait site. CH_3Hg averaged 0.20 pM in the Beaufort Sea ice, but rose to 1.35 pM in the McClure Strait. Percent CH_3Hg ranged from 2.3-40.9%, peaking in the mid to bottom sections of the ice, possibly suggesting in situ methylation. In the Southern Ocean, Cossa et al. (2011) also measured higher Hg_T concentrations at the surface of ice cores with average concentrations at depth around 3 pM. CH_3Hg concentrations were relatively consistent throughout the core, with concentrations up to almost 0.4 pM. Clearly, while there is the possibility of higher concentrations in coastal ice regions based on the collections in both the Arctic and Antarctic discussed above, our data do not suggest that these high concentrations persist in ice collected further offshore. These differences suggest that collections in the coastal Arctic should not be extrapolated to the central basin as these data are not likely representative of the Arctic open waters.

Previous measurements in surface snow have focused on periods following AMDEs given the dramatic changes that can occur due to deposition of oxidized Hg, resulting in concentrations that are much higher than those measured here. Studies indicate that a significant portion of the Hg deposited in quickly reduced and emitted back to the atmosphere (Kirk et al., 2012; 2006; Steffen et al., 2015). St Louis et al. (2007), for example, measured decreasing concentrations in the snowpack in Alert into June, with Hg_T concentrations dropping below 5 pM later in the season. CH_3Hg concentrations also fell below 1 pM, especially in the base of the snowpack. Percent CH_3Hg was low at the surface (0.4 ± 0.5 %), but increased in the depth hoar snow (3.6 ± 7.0 %). On the Hudson Bay, Kirk et al. (2006) measured concentrations of Hg_T in surface snow as high as 3.30 nM in the spring of 2003, but concentrations dropped to ~25 pM within days. Lu et al. (2001) measured Hg_T in sea ice snow in the Beaufort Sea, finding concentrations as low as ~13 pM between November and December, with concentrations rising throughout the spring. Chaulk et al. (2011) measured Hg_T concentrations less than 5 pM in snow from the coastal Beaufort Sea, with higher peaks due to atmospheric deposition. Our Hg_T

concentrations (3.6 ± 1.3 pM) indicate Hg levels in surface snow in the Central Basin in the late summer and fall are even lower than many coastal locations. These concentrations are valuable in understanding the importance of surface snow and ice as a source of Hg to the biosphere. The low concentrations observed are a result of the release of the Hg that had accumulared over the previous AMDEs. Melting snowpack releases water soluble oxidized Hg(II) to the surface ocean, while Hg^0 can be volatilized back to the atmosphere following the reduction of Hg(II) (Chaulk et al., 2011; Lu et al., 2001).

Mass balance

Due to temporal variability during the times of the year not covered by the cruise, especially given the potentially high exchange during polar sunrise where AMDEs and Hg deposition are heightened, the estimates of wet and dry deposition were calculated on a monthly basis to represent values during the time of the cruise. The overall low precipitation (340 mm yr^{-1}; Serreze et al., 2006) at high latitudes results in relatively low wet deposition of Hg to the Arctic. Monthly wet deposition, calculated from the measured concentrations, Arctic Ocean surface area, and yearly precipitation, is estimated to be 7.6 mol of CH_3Hg and 1.0 kmol of Hg_T. Based on the measurements in aerosols and an estimated dry deposition velocity of 0.5 cm s^{-1} (Holmes et al., 2009), given that there appeared to be mainly fine particulate aerosols, 1.0 mol of CH_3Hg and 0.24 kmol of Hg_T were deposited per month via dry aerosol deposition. Similarly, Hg_R was deposited at a rate of 1.5 kmol mth^{-1}. The total atmospheric deposition to the surface Arctic Ocean was thus estimated as 8.6 mol mth^{-1} CH_3Hg and 2.7 kmol mth^{-1} Hg_T. Wet deposition represented 88% of the CH_3Hg flux and 38% of the Hg_T flux, with dry deposition making up the remainder. In other parts of the world, greater precipitation typically results in a greater importance of wet deposition to the Hg_T flux (e.g., Gichuki and Mason, 2014). These calculations also did not include reactive gaseous CH_3Hg (CH_3Hg_R) which was not measured, but previous studies have shown the it might constitute up to 25% of Hg_R (Baya et al., 2015). Even at a much lower percentage, CH_3Hg_R could dominate dry deposition and thus decrease the importance of wet deposition. Atmospheric inputs of CH_3Hg and Hg_T were estimated to be much higher by Soerensen et al. (2016), with values of 3.3 kmol mth^{-1} CH_3Hg and 12.5 kmol mth^{-1} Hg_T. Their estimate of CH_3Hg atmospheric deposition was much greater in part due to the inclusion of CH_3Hg produced by the degradation of dimethylmercury ($(CH_3)_2Hg$) in the atmosphere. However, recent work in the Arctic suggests that evasional fluxes of $(CH_3)_2Hg$ from the surface ocean have been overestimated in the Soerensen et al. model (S. Jonsson, personal comm.).

For gas exchange, applying the overall average calculated Hg^0 evasion rate to the entire Arctic (8.2 pmol m^{-2} h^{-1}) is unreasonable because evasion does not occur under ice where predicted fluxes are greatest. Applying the average Hg^0 flux in open waters (2.1 pmol m^{-2} h^{-1}) to the average area of open water (40.3 % open water; 11.1 x 10^6 km^2 total area with 6.65 x 10^6 km^2 ice coverage; NSIDC, 2016; Soerensen et al., 2016), we calculate an evasion of 6.8 kmol mth^{-1}. This flux is about five times lower than the average monthly flux reported by Soerensen et al. (2016) (35 kmol mth^{-1}). Although deposition and evasion were similar in magnitude in our study, our estimate does not account for evasion of Hg deposited on snow and ice cover. Soerensen et al. (2016) estimated that atmospheric deposition and snow and ice melt inputs were similar in magnitude. Accounting for this melt term, we would expect to find greater evasion than atmospheric input indicating the need for coastal and riverine inputs, as well as water transport from the Atlantic and Pacific, to make up the difference.

5 Conclusions

Dissolved and atmospheric Hg^0 concentrations, measured continuously at high temporal resolution in Arctic Ocean, have further contributed to our understanding of the air-sea exchange of Hg in the Arctic. Our data suggest that sea ice plays a large role in the accumulation of Hg^0_{diss} in the surface Arctic Ocean. While concentrations averaged 32 ± 30 fM in open water, they rose as high as 544 fM under contiguous ice. This increase confirms the previous observations of the accumulation of Hg^0_{diss} in the Arctic during periods of ice coverage. This trend was attributed to sea ice acting as a barrier for Hg^0 air-sea exchange, and the continued net formation of Hg^0, even under the ice in the absence of elevated radiation levels. Because variations in atmospheric Hg^0 concentrations (averaging 1.2 ± 0.1 ng m^{-3}) were relatively small, wind speed and Hg^0_{diss} concentrations were the major drivers of the predicted Hg^0 evasional flux.

Measurements of CH_3Hg and Hg_T in precipitation and aerosols in the central Arctic also substantially add to our previous knowledge, as much of the previous research has focused on measurements made from or near land. Our results suggest that deposition and aerosol concentrations in the open waters of the Arctic are much lower than in coastal regions and the Canadian Arctic Archipelago. Levels of Hg in fine and bulk aerosols were similar, suggesting that the uptake of Hg_R into aerosols was not an important mechanism for Hg_R removal during the time of the cruise.

Ice core and surface snow measurements also helped quantify the amount of Hg that could be entering the ocean through ice melt in the central Arctic. Initially, melting sea ice in a warming climate will likely lead to increased Hg^0 evasion, resulting in decreased Hg levels in the surface Arctic Ocean. Subsaturated concentrations in other parts of the Arctic however suggest an eventual decrease in evasion in the absence of sea ice. These additional insights and high resolution measurements will help to further refine global and regional Hg models, improving their ability to predict future changes in Hg transport and transformations within diverse marine ecosystems. Future studies focusing on air-sea exchange dynamics in marginal ice zones will also aid in understanding the extent of Hg^0 evasion in open leads and polynyas in the Arctic.

Acknowledgements

We would like to thank the captain and crew of the ship, the USCGC *Healy*, as well as our colleagues on the U.S. Arctic GEOTRACES cruise, especially: Steve Brooks and Chris Moore for Hg^0 measurements aboard the ship and at Barrow, Alaska; Cliff Buck, Pete Morton, and Brent Summers for collection of the atmospheric samples; Ana Aguilar-Islas, Rob Rember, and Bill Landing for ice core, snow, and melt pond sampling; and Carl Lamborg, Katlin Bowman, and Alison Agather for sample preparation and storage. We would also like to thank Prentiss Balcom for pre-cruise preparation including the underway sampling equipment. This study was funded by the National Science Foundation (NSF) Chemical Oceanography Program through grant #1434998, and was part of the PhD thesis of Brian DiMento.

Appendix A. Supporting Information

Discrete vs. Underway Samples

Hg^0_{diss} concentrations were also measured in discrete samples (collected in Go-Flo bottles) using traditional methods (Lamborg et al., 2012) at each station on the cruise. These data

were compared to average Hg^0_{diss} concentrations measured using the underway system while the ship was on the corresponding station. While the slope was close to 1 and values were significantly correlated ($R^2 = 0.42$, $p < 0.05$), the agreement was not as strong as found in previous studies which showed good agreement between the two methods (Andersson et al., 2008a; 2008c; Soerensen et al., 2013). Poor agreement here is likely due to the high variability in concentrations observed under the ice, and possibly from evasion in open leads in the ice caused naturally or by the movement of the ship while on station. As noted in the methods section, we did not include the "underway" data while on station in our analysis because of concerns about its reliability. Discrete samples also represent a single measurement taken while on station, so they are unable to capture the variability observed in the continuous measurements. These samples also were not consistently collected at the same depth as underway samples, potentially adding to the discrepancies between the two measurement methods as they may not have sampled the same water masses where the mixed layer depth was shallow (<10m).

Ancillary Data

Surface waters encountered on the cruise were characterized by higher salinity Pacific water moving over the continental shelf from the Bering Sea through the Bering Strait to the Chukchi Sea, followed by waters of lower salinity and temperature of the Polar Mixed Layer, starting at the continental shelf break and continuing to the North Pole. The sea surface temperature (SST), wind speed, salinity and fluorescence along the cruise track are shown in Fig. S1. A salinity minimum was observed at the MIZ where ice melt further decreased the salinity. Fluorescence was highest in the coastal waters off the coast of Alaska. Average wind speed rose slightly over the course of the cruise, with intermittent peaks over 20 m s^{-1} observed in the central Arctic (north of 80 °N).

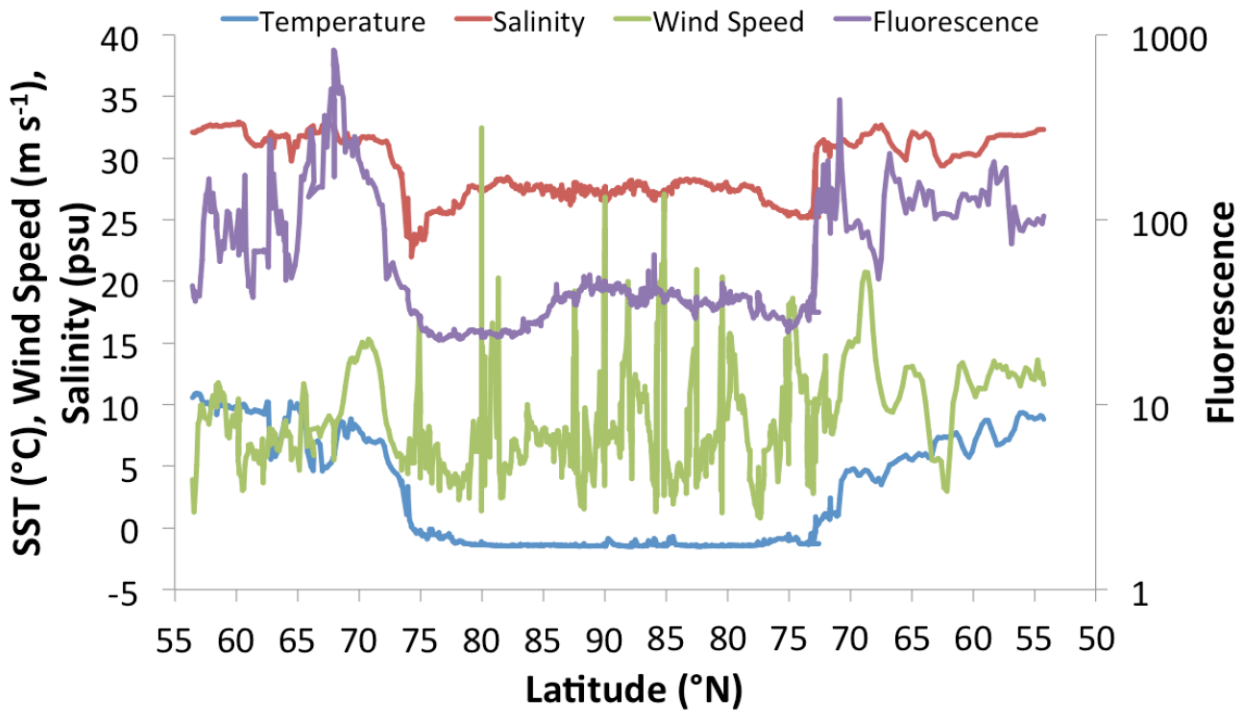

640

641 **Fig. S1.** Ancillary data—sea surface temperature (SST), salinity, wind speed, and fluorescence—
642 on the U.S. Arctic GEOTRACES cruise track.

643 Comparing Hg^0_{diss} concentrations to sea surface salinity, temperature and fluorescence, as
644 well as Hg^0_{atmos} (Fig. S2) reveals that Hg^0_{diss} concentrations are highest at median salinities and
645 Hg^0_{atmos} levels as well as the lowest temperatures and fluorescence values. These parameters
646 correspond to the polar mixed layer. The lowest salinities represent the MIZ, while the high
647 salinities represent the Pacific water at lower latitudes. Hg^0_{diss} appears to be normally distributed
648 versus Hg^0_{atmos}. If evasion could occur in ice-covered regions, we would expect to see higher
649 Hg^0_{atmos} concentrations as Hg^0_{diss} values increased.

650

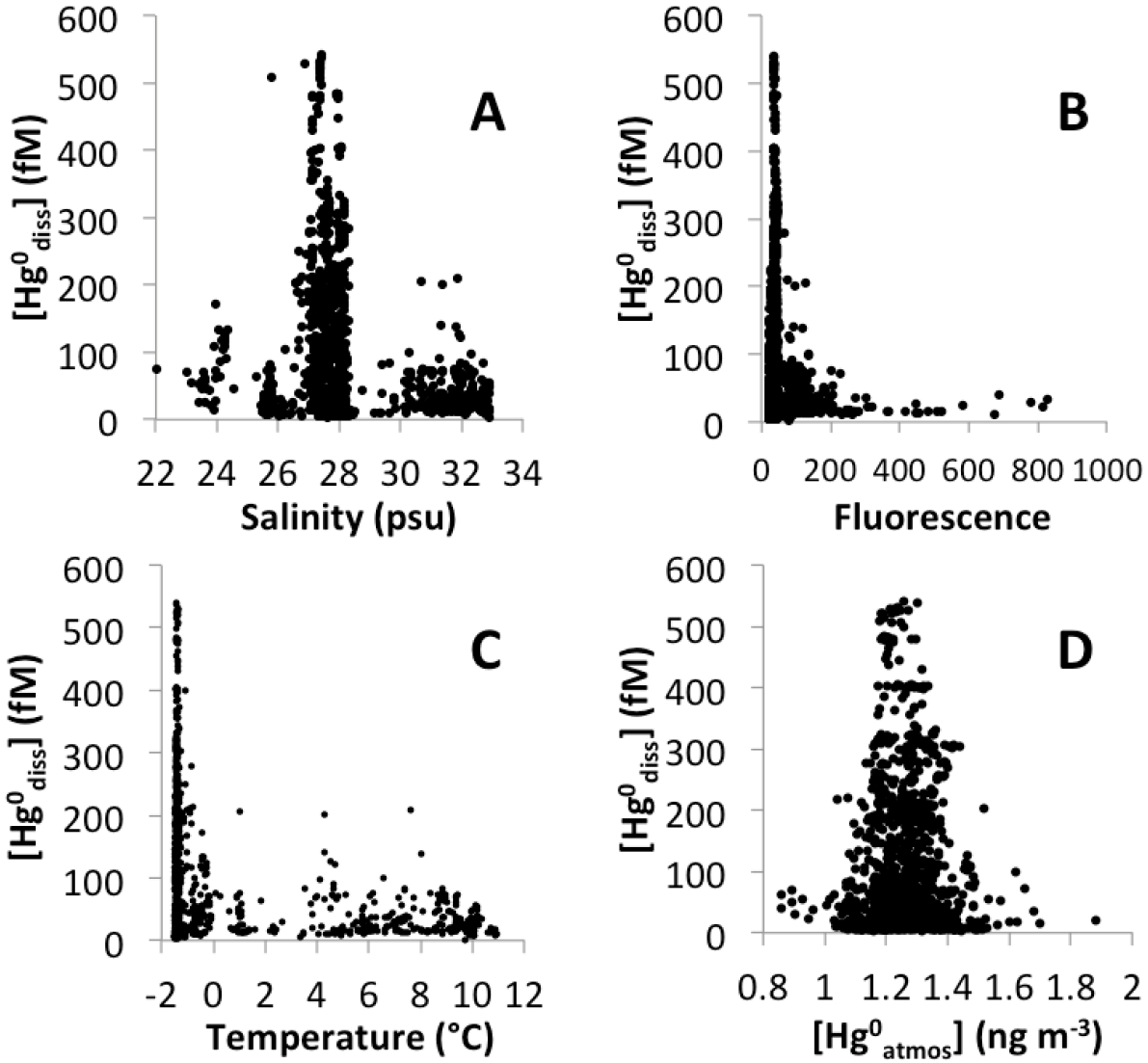

651

652 **Fig. S2.** Relationships between dissolved Hg^0 (Hg^0_{diss}) and sea surface salinity (A), fluorescence
653 (B), temperature (C), and Hg^0 in air (D) along the U.S. Arctic GEOTRACES cruise track.

654

655 ***Aerosols and Precipitation***

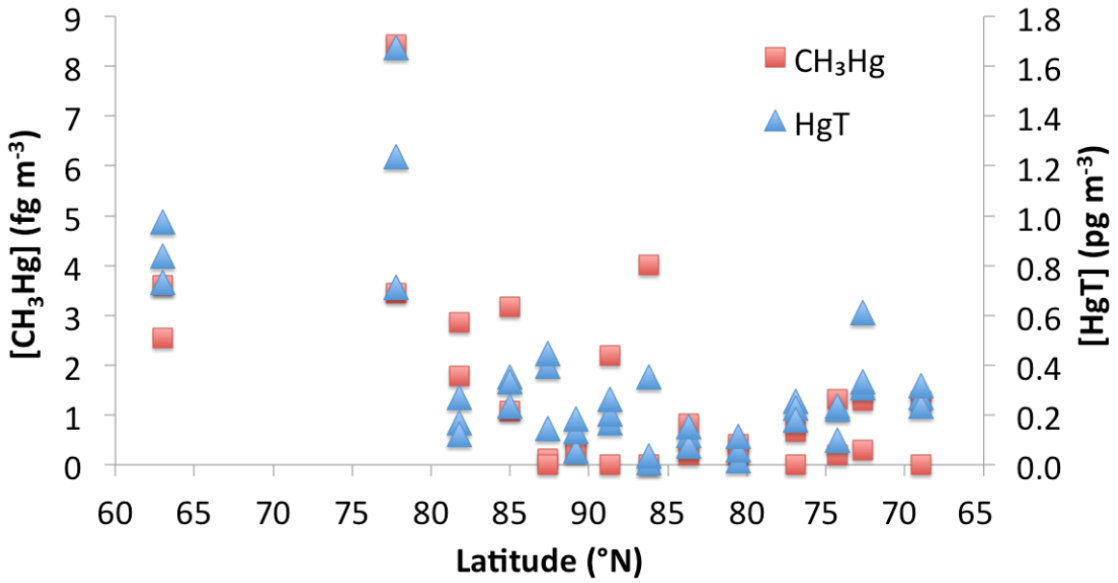

656

657 **Fig. S3.** Aerosol particulate methyl (CH_3Hg_P) total Hg (Hg_P) concentrations. The sample
658 latitudes represent the average latitude of each deployment. The first two deployments were
659 longer with a small gap in collection in between, covering 56.1 – 69.9 °N and 75.6 – 78.0 °N.

660

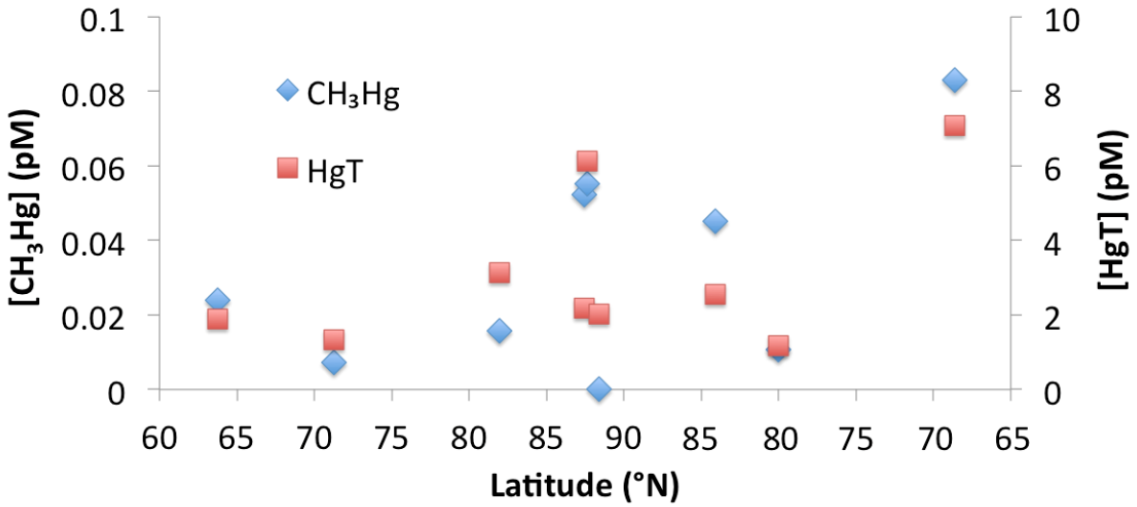

661

662 **Fig. S4.** Methyl (CH_3Hg) and total Hg (Hg_T) concentrations in rain. The sample latitudes
663 represent the average latitude of each deployment.

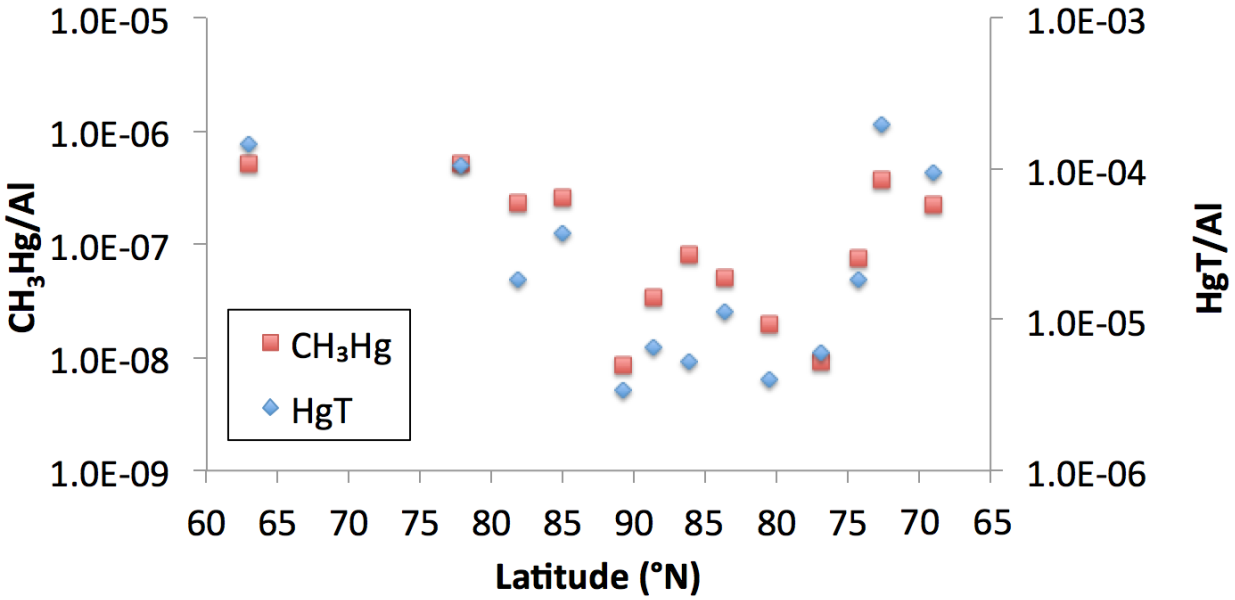

664

665 **Fig. S5.** Mass ratios of CH_3Hg and HgT to aluminum (Al) in aerosols.

666 ***Percent Saturation***

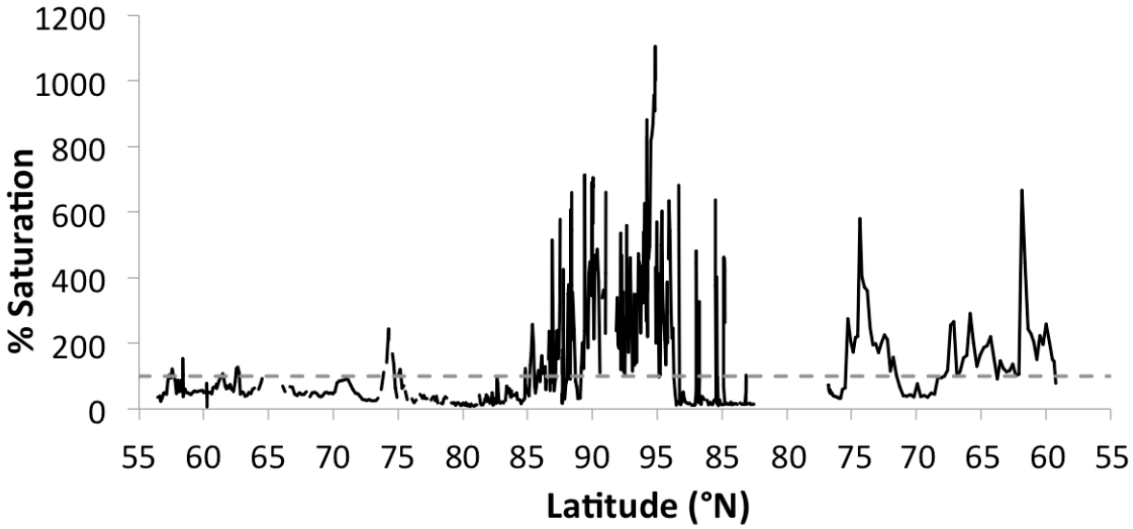

667

668 **Fig. S6.** Percent saturation of dissolved Hg^0 (Hg^0_{diss}) in the surface ocean along the U.S. Arctic
669 GEOTRACES cruise track.

670

671 ***Early Cruise Data***

672 The Hg^0_{diss} concentration during the early stages of the cruise, from day 2 to 10 of the
673 cruise (and especially when further from anthropogenic and terrestrial influences), showed
674 evidence of diurnal variations (Fig. S7). Concentrations were positively and significantly
675 correlated with photosynthetically active radiation (PAR) ($R^2 = 0.22$, $p < 0.05$), indicating

676 production of Hg^0 and reoxidation of Hg^0 or loss by evasion during the course of a day.
677 Production has been observed to be due both abiotic (photochemical) and biotic light-induced
678 processes (Amyot et al., 1997). Because the on-station data were not considered, there were too
679 many gaps in the data to continue this correlation further into the ice-free period. This
680 phenomenon has been observed previously in other ocean water bodies (e.g., Amyot et al., 1997;
681 1994; Andersson et al., 2007a; Ci et al., 2016; 2011; Fantozzi et al., 2007; Sommar et al., 2007).

682

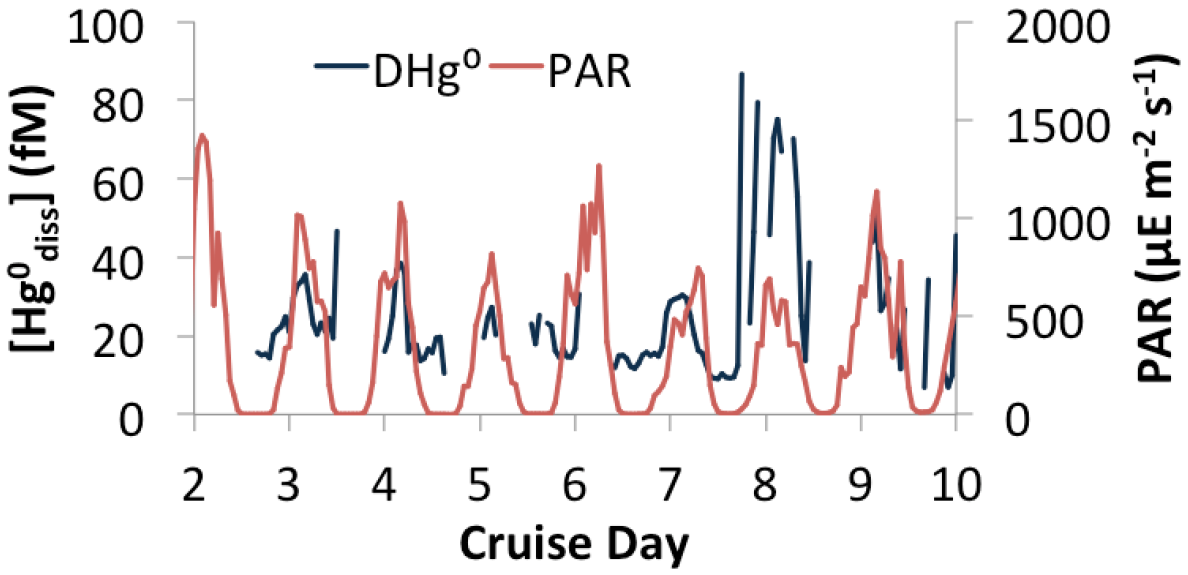

683

684 **Fig. S7.** Dissolved Hg^0 concentrations ($[Hg^0_{diss}]$) and photosynthetically active radiation (PAR)
685 during the first ten days of the U.S. Arctic GEOTRACES cruise.

686 Looking more closely at the data obtained during the early stages of the cruise (when the
687 ship was in open water and the MIZ on the western leg) reveals finer scale variations in Hg^0_{diss}
688 concentrations and fluxes that provide further insight into its cycling (Fig. S8). Sea surface
689 temperature and salinity were relatively constant until the MIZ was reached, where the
690 temperature and salinity dropped to a minimum. Where ice cover began to increase at 75 °N, a
691 brief increase in Hg^0_{diss} was observed along with a small decline in Hg^0_{atmos}. This trend resembles
692 an AMDE (Cobbett et al., 2007), and coincides with increase aerosol particulate Hg measured
693 over the same period (Fig. S3). Following this decline, atmospheric Hg^0 concentrations rose in
694 the MIZ, possibly indicating the evasion of Hg^0 from the sea surface as the remaining ice melted.
695 At 80 °N, after Hg^0_{diss} concentrations had returned to a background level, the effect of increased
696 winds is evident in the large predicted (negative) flux of Hg^0 from the atmosphere into the ocean.

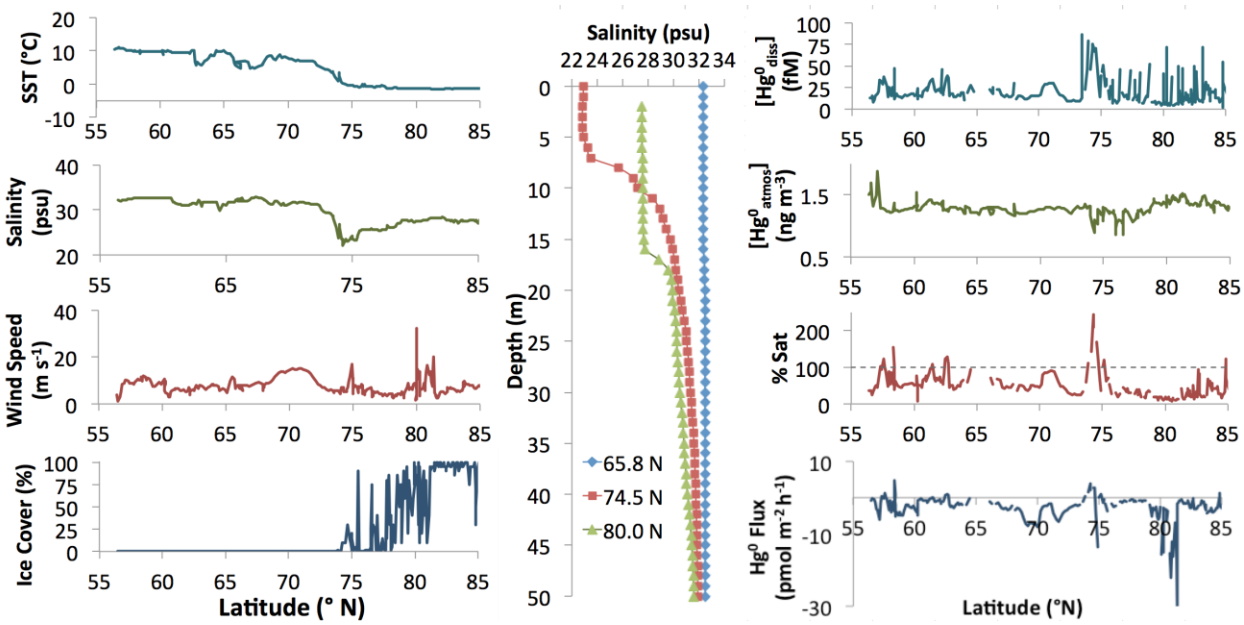

Fig. S8. Hg^0 and ancillary data profiles from the western leg open water and marginal ice zone (MIZ) of the U.S. Arctic GEOTRACES cruise. Sea surface temperature (SST) (A), salinity (B), wind speed (C) and ice cover (D). Salinity profiles (E) from the early stage of the cruise as well as the beginning and end of the MIZ. Dissolved Hg^0 ($[Hg^0_{diss}]$) (F) and atmospheric Hg^0 ($[Hg^0_{atmos}]$) (G) concentrations, along with the percent saturation of Hg^0 in surface seawater (H) and the predicted Hg^0 flux out of the ocean (I).

References

AMAP, 2011. AMAP Assessment 2011: Mercury in the Arctic. Arctic Monitoring and Assessment Programme, Oslo, Norway.

Amyot, M., Gill, G.A., Morel, F.M.M., 1997. Production and Loss of Dissolved Gaseous Mercury in Coastal Seawater. Environ. Sci. Technol. 31, 3606–3611. doi:10.1021/es9703685

Amyot, M., McQueen, D.J., Mierle, G., Lean, D.R.S., 1994. Sunlight-Induced Formation of Dissolved Gaseous Mercury in Lake Waters. Environ. Sci. Technol. 28, 2366–2371. doi:10.1021/es00062a022

Andersson, M.E., Gårdfeldt, K., Wängberg, I., 2008a. A description of an automatic continuous equilibrium system for the measurement of dissolved gaseous mercury. Anal Bioanal Chem 391, 2277–2282. doi:10.1007/s00216-008-2127-4

Andersson, M.E., Gårdfeldt, K., Wängberg, I., Sprovieri, F., Pirrone, N., Lindqvist, O., 2007a. Seasonal and daily variation of mercury evasion at coastal and off shore sites from the Mediterranean Sea. Marine Chemistry 104, 214–226. doi:10.1016/j.marchem.2006.11.003.

Andersson, M.E., Gårdfeldt, K., Wängberg, I., Sprovieri, F., Pirrone, N., Lindqvist, O., 2007b. Seasonal and daily variation of mercury evasion at coastal and off shore sites from the Mediterranean Sea. Marine Chemistry 104, 214–226. doi:10.1016/j.marchem.2006.11.003

Andersson, M.E., Gårdfeldt, K., Wängberg, I., Strömberg, D., 2008b. Determination of Henry's law constant for elemental mercury. Chemosphere 73, 587–592. doi:10.1016/j.chemosphere.2008.05.067

Andersson, M.E., Sommar, J., Gårdfeldt, K., Lindqvist, O., 2008c. Enhanced concentrations of dissolved gaseous mercury in the surface waters of the Arctic Ocean. Marine Chemistry 110, 190–194. doi:10.1016/j.marchem.2008.04.002

Ariya, P.A., Dastoor, A.P., Amyot, M., Schroeder, W.H., BARRIE, L., ANLAUF, K., Raofie, F., Ryzhkov, A., DAVIGNON, D., LALONDE, J., Steffen, A., 2004. The Arctic: a sink for mercury. Tellus B 56, 397–403. doi:10.1111/j.1600-0889.2004.00118.x

Bais, A.F., Tourpali, K., Kazantzidis, A., Akiyoshi, H., Bekki, S., Braesicke, P., Chipperfield, M.P., Dameris, M., Eyring, V., Garny, H., Iachetti, D., Jöckel, P., Kubin, A., Langematz, U., Mancini, E., Michou, M., Morgenstern, O., Nakamura, T., Newman, P.A., Pitari, G., Plummer, D.A., Rozanov, E., Shepherd, T.G., Shibata, K., Tian, W., Yamashita, Y., 2011. Projections of UV radiation changes in the 21st century: impact of ozone recovery and cloud effects. Atmos. Chem. Phys. 11, 7533–7545. doi:10.5194/acp-11-7533-2011

Baya, P.A., Gosselin, M., Lehnherr, I., St Louis, V.L., Hintelmann, H., 2015. Determination of Monomethylmercury and Dimethylmercury in the Arctic Marine Boundary Layer. Environ. Sci. Technol. 49, 223–232. doi:10.1021/es502601z

Beattie, S.A., Armstrong, D., Chaulk, A., Comte, J., Gosselin, M., Wang, F., 2014. Total and Methylated Mercury in Arctic Multiyear Sea Ice. Environ. Sci. Technol. 48, 5575–5582. doi:10.1021/es5008033

Bekryaev, R.V., Polyakov, I.V., Alexeev, V.A., 2010. Role of Polar Amplification in Long-Term Surface Air Temperature Variations and Modern Arctic Warming. J. Climate 23, 3888–3906. doi:10.1175/2010JCLI3297.1

Bintanja, R., Graversen, R.G., Hazeleger, W., 2011. Arctic winter warming amplified by the thermal inversion and consequent low infrared cooling to space. Nature Geoscience 4, 758–761. doi:10.1038/ngeo1285

Braune, B., Chételat, J., Amyot, M., Brown, T., Clayden, M., Evans, M., Fisk, A., Gaden, A., Girard, C., Hare, A., Kirk, J., Lehnherr, I., Letcher, R., Loseto, L., Macdonald, R., Mann, E., McMeans, B., Muir, D., O'Driscoll, N., Poulain, A., Reimer, K., Stern, G., 2015. Mercury in the marine environment of the Canadian Arctic: Review of recent findings. Science of the Total Environment, The 509-510, 67–90. doi:10.1016/j.scitotenv.2014.05.133

Cavalieri, D.J., Parkinson, C.L., 2012. Arctic sea ice variability and trends, 1979-2010. The Cryosphere 6, 881–889. doi:10.5194/tc-6-881-2012

Chaulk, A., Stern, G.A., Armstrong, D., Barber, D.G., Wang, F., 2011. Mercury Distribution and Transport Across the Ocean−Sea-Ice−Atmosphere Interface in the Arctic Ocean. Environ. Sci. Technol. 45, 1866–1872. doi:10.1021/es103434c

Ci, Z., Zhang, X., Wang, Z., 2016. Air–sea exchange of gaseous mercury in the tropical coast (Luhuitou fringing reef) of the South China Sea, the Hainan Island, China. Environmental Science and Pollution Research 1–7. doi:10.1007/s11356-016-6346-5

762 Ci, Z., Zhang, X., Wang, Z., 2011. Elemental mercury in coastal seawater of Yellow Sea, China:
763 Temporal variation and air-sea exchange. Atmospheric Environment 45, 183–190.
764 doi:10.1016/j.atmosenv.2010.09.025

765 Clarkson, T.W., Magos, L., 2006. The Toxicology of Mercury and Its Chemical Compounds.
766 Critical Reviews in Toxicology 36, 609–662. doi:10.1080/10408440600845619

767 Cobbett, F.D., Steffen, A., Lawson, G., Van Heyst, B.J., 2007. GEM fluxes and atmospheric
768 mercury concentrations (GEM, RGM and Hgp) in the Canadian Arctic at Alert, Nunavut,
769 Canada (February–June 2005). Atmospheric Environment 41, 6527–6543.
770 doi:10.1016/j.atmosenv.2007.04.033

771 Corbitt, E.S., Jacob, D.J., Holmes, C.D., Streets, D.G., Sunderland, E.M. 2011. Global Source-
772 Receptor Relationships for Mercury Deposition Under Present-Day and 2050 Emissions
773 Scenarios. Environ. Sci. Technol. 45, 10477-10484.

774 Cossa, D., Heimbürger, L.E., Lannuzel, D., Rintoul, S.R., Butler, E.C.V., Bowie, A.R., Averty,
775 B., Watson, R.J., Remenyi, T., 2011. Mercury in the southern ocean. Geochimica et
776 Cosmochimica Acta 75, 4037–4052. doi:10.1016/j.gca.2011.05.001

777 Dastoor, A., Ryzhkov, A., Durnford, D., Lehnherr, I., Steffen, A., Morrison, H., 2015.
778 Atmospheric mercury in the Canadian Arctic. Part II: Insight from modeling. Science of the
779 Total Environment, The 509-510, 16–27. doi:10.1016/j.scitotenv.2014.10.112

780 Dastoor, A.P., Durnford, D.A., 2014. Arctic Ocean: Is It a Sink or a Source of Atmospheric
781 Mercury? Environ. Sci. Technol. 48, 1707–1717. doi:10.1021/es404473e

782 Driscoll, C.T., Mason, R.P., Chan, H.M., Jacob, D.J., Pirrone, N., 2013. Mercury as a Global
783 Pollutant: Sources, Pathways, and Effects. Environ. Sci. Technol. 47, 4967–4983.
784 doi:10.1021/es305071v

785 Fanning, K.A., Torres, L.M., 1991. ^{222}Rn and ^{226}Ra: indicators of sea-ice effects on air-sea gas
786 exchange. Polar Research 10, 51-58. doi:10.1111/j.1751-8369.1991.tb00634.x

787 Fantozzi, L., Ferrara, R., Frontini, F.P., Dini, F., 2007. Factors influencing the daily behaviour of
788 dissolved gaseous mercury concentration in the Mediterranean Sea. Marine Chemistry 107,
789 4–12. doi:10.1016/j.marchem.2007.02.008

790 Fisher, J.A., Jacob, D.J., Soerensen, A.L., Amos, H.M., Corbitt, E.S., Streets, D.G., Wang, Q.,
791 Yantosca, R.M., Sunderland, E.M., 2013. Factors driving mercury variability in the Arctic
792 atmosphere and ocean over the past 30 years. Global Biogeochem. Cycles 27, 1226–1235.
793 doi:10.1002/2013GB004689

794 Fitzgerald, W.F., Lamborg, C.H., Hammerschmidt, C.R., 2007. Marine biogeochemical cycling
795 of mercury. Chem. Rev. 107, 641–662. doi:10.1021/cr050353m

796 Gichuki, S.W., Mason, R.P., 2014. Wet and dry deposition of mercury in Bermuda. Atmospheric
797 Environment 87, 249–257. doi:10.1016/j.atmosenv.2014.01.025

798 Gionfriddo, C.M., Tate, M.T., Wick, R.R., Schultz, M.B., Zemla, A., Thelen, M.P., Schofield,
799 R., Krabbenhoft, D.P., Holt, K.E., Moreau, J.W., 2016. Microbial mercury methylation in
800 Antarctic sea ice. Nature Microbiology 1–12. doi:10.1038/nmicrobiol.2016.127

Hammerschmidt, C.R., Fitzgerald, W.F., 2005. Methylmercury in Mosquitoes Related to Atmospheric Mercury Deposition and Contamination. Environ. Sci. Technol. 39, 3034–3039. doi:10.1021/es0485107

Hammerschmidt, C.R., Fitzgerald, W.F., 2006. Bioaccumulation and trophic transfer of methylmercury in Long Island Sound. Arch Environ Contam Toxicol 51, 416–424. doi:10.1007/s00244-005-0265-7

Holmes, C.D., Jacob, D.J., Mason, R.P., Jaffe, D.A., 2009. Sources and deposition of reactive gaseous mercury in the marine atmosphere. Atmospheric Environment 43, 2278–2285. doi:10.1016/j.atmosenv.2009.01.051

Kim, H., Rhee, T.S., Hahm, D., Hwang, C.Y., Yang, J., Han, S., 2016. Contrasting distributions of dissolved gaseous mercury concentration and evasion in the North Pacific Subarctic Gyre and the Subarctic Front. Deep-Sea Research Part I 110, 90–98. doi:10.1016/j.dsr.2016.02.001

Kirk, J.L., Lehnherr, I., Andersson, M., Braune, B.M., Chan, L., Dastoor, A.P., Durnford, D., Gleason, A.L., Loseto, L.L., Steffen, A., St Louis, V.L., 2012. Mercury in Arctic marine ecosystems: Sources, pathways and exposure. Environmental Research 119, 64–87. doi:10.1016/j.envres.2012.08.012

Kirk, J.L., Louis, V.S., Sharp, M.J., 2006. Rapid reduction and reemission of mercury deposited into snowpacks during atmospheric mercury depletion events at Churchill, Manitoba, Canada. Environmental science & … 40, 7590–7596. doi:10.1021/es061299

Kuss, J., Zülicke, C., Pohl, C., Schneider, B., 2011. Atlantic mercury emission determined from continuous analysis of the elemental mercury sea-air concentration difference within transects between 50°N and 50°S. Global Biogeochem. Cycles 25, n/a–n/a. doi:10.1029/2010GB003998

Lalonde, J.D., Poulain, A.J., Amyot, M., 2002. The Role of Mercury Redox Reactions in Snow on Snow-to-Air Mercury Transfer. Environ. Sci. Technol. 36, 174–178. doi:10.1021/es010786g

Lamborg, C.H., Bowman, K., Hammerschmidt, C.R., Gilmour, C., Munson, K., Selin, N., Tseng, C.-M., 2014. Mercury in the Anthropocene Ocean. oceanog 27, 76–87. doi:10.5670/oceanog.2014.11

Lamborg, C.H., Hammerschmidt, C.R., Gill, G.A., Mason, R.P., Gichuki, S., 2012. An intercomparison of procedures for the determination of total mercury in seawater and recommendations regarding mercury speciation during GEOTRACES cruises. Limnol. Oceangr. Methods 10, 90–100. doi:10.4319/lom.2012.10.90

Landis, M.S., Stevens, R.K., Schaedlich, F., Prestbo, E.M., 2002. Development and Characterization of an Annular Denuder Methodology for the Measurement of Divalent Inorganic Reactive Gaseous Mercury in Ambient Air. Environ. Sci. Technol. 36, 3000–3009. doi:10.1021/es015887t

Laurier, F., Mason, R.P., Whalin, L., Kato, S., 2003. Reactive gaseous mercury formation in the North Pacific Ocean's marine boundary layer: A potential role of halogen chemistry. Journal

841 of Geophysical Research 108. doi:10.1029/2003JD003625

842 Lehnherr, I., St. Louis, V.L., Emmerton, C.A., Barker, J.D., Kirk, J.L. (2012) Methylmercury
843 cycling in High Arctic wetland ponds: Sources and sinks. Environ. Sci. Technol. 46, 10514-
844 10522.

845 Lindberg, S., Bullock, R., Ebinghaus, R., Engstrom, D., Feng, X., Fitzgerald, W., Pirrone, N.,
846 Prestbo, E., Seigneur, C., Panel on Source Attribution of Atmospheric Mercury, 2007. A
847 synthesis of progress and uncertainties in attributing the sources of mercury in deposition.
848 Ambio 36, 19–32.

849 Lindberg, S.E., Brooks, S., Lin, C.J., Scott, K., Meyers, T., Chambers, L., Landis, M., Stevens,
850 R., 2001. Formation of Reactive Gaseous Mercury in the Arctic: Evidence of Oxidation of
851 Hg° to Gas- Phase Hg-II Compounds... Water, Air, & Soil Pollution: Focus 1, 295–302.
852 doi:10.1023/A:1013171509022

853 Loose, B., McGillis, W.R., Schlosser, P., Perovich, D., Takahashi, T., 2009. Effects of freezing,
854 growth, and ice cover on gas transport processes in laboratory seawater experiments.
855 Geophysical Research Letters 36, L05603. doi:10.1029/2008GL036318
856
857 Loose, B., Miller, L.A., Elliott, S., Papakyriakou, T., 2011. Sea ice biogeochemistry and material
858 transport across the frozen interface. Oceanography 24, 202-218.

859 Lu, J. Y., Schroeder, W. H., Barrie, L. A., Steffen, A., Welch, H. E., Martin, K., Lockhart, L.,
860 Hunt, R. V., Boila, G., Richter, A., 2001. Magnification of atmospheric mercury deposition
861 to polar regions in springtime: the link to tropospheric ozone depletion chemistry.
862 Geosphysical Research Letters 28, 3219-3222. doi: 10.1029/2000GL012603

863 Macdonald, R.W., Harner, T., Fyfe, J., 2005. Recent climate change in the Arctic and its impact
864 on contaminant pathways and interpretation of temporal trend data. Science of The Total
865 Environment 342, 5–86. doi:10.1016/j.scitotenv.2004.12.059

866 Mahaffey, K.R., Sunderland, E.M., Chan, H.M., Choi, A.L., Grandjean, P., Mariën, K., Oken, E.,
867 Sakamoto, M., Schoeny, R., Weihe, P., Yan, C.-H., Yasutake, A., 2011. Balancing the
868 benefits of n-3 polyunsaturated fatty acids and the risks of methylmercury exposure from
869 fish consumption. Nutrition Reviews 69, 493–508. doi:10.1111/j.1753-4887.2011.00415.x

870 Mason, R.P., Choi, A.L., Fitzgerald, W.F., Hammerschmidt, C.R., Lamborg, C.H., Soerensen,
871 A.L., Sunderland, E.M., 2012. Mercury biogeochemical cycling in the ocean and policy
872 implications. Environmental Research 119, 101–117. doi:10.1016/j.envres.2012.03.013

873 Mason, R.P., Hammerschmidt, C.R., Lamborg, C.H., Bowman, K.L., Swarr, G.J., Shelley, R.U.,
874 2017. The air-sea exchange of mercury in the low latitude Pacific and Atlantic Oceans. Deep
875 Sea Research Part I: Oceanographic Research Papers Under Review.

876 Mason, R.P., Lawson, N.M., Lawrence, A.L., Leaner, J.J., Lee, J.G., Sheu, G.-R., 1999. Mercury
877 in the Chesapeake Bay. Marine Chemistry 65, 77–96. doi:10.1016/S0304-4203(99)00012-2

878 Mason, R.P., Rolfhus, K.R., Fitzgerald, W.F., 1998. Mercury in the North Atlantic. Marine
879 Chemistry 61, 37–53. doi:10.1016/S0304-4203(98)00006-1

880 Morton, P.L., Landing, W.M., Hsu, S.-C., Milne, A., Aguilar-Islas, A.M., Baker, A.R., Bowie,

A.R., Buck, C.S., Gao, Y., Gichuki, S., Hastings, M.G., Hatta, M., Johansen, A.M., Losno, R., Mead, C., Patey, M.D., Swarr, G., Vandermark, A., Zamora, L.M., 2013. Methods for the sampling and analysis of marine aerosols: results from the 2008 GEOTRACES aerosol intercalibration experiment. Limnol. Oceangr. Methods 11, 62–78. doi:10.4319/lom.2013.11.62

National Snow and Ice Data Center (NSIDC), 2016. Antarctic Sea Ice Extent [WWW Document]. httpnsidc.orgarcticseaicenewscharctic-interactive-sea-ice-graph. URL (accessed 12.24.16).

NOAA Climate.gov. [NOAAClimate]. (2016, December 13). *Arctic sea ice growing younger, thinner.* Retrieved from https://www.youtube.com/watch?v=c6jX9URzZWg

O'Driscoll, N.J., Siciliano, S.D., Lean, D.R.S., Amyot, M., 2006. Gross Photoreduction Kinetics of Mercury in Temperate Freshwater Lakes and Rivers: Application to a General Model of DGM Dynamics. Environ. Sci. Technol. 40, 837–843. doi:10.1021/es051062y

Outridge, P.M., Macdonald, R.W., Wang, F., Stern, G.A., Dastoor, A.P., 2008. A mass balance inventory of mercury in the Arctic Ocean. Environ. Chem. 5, 89–23. doi:10.1071/EN08002

Parkinson, C.L., Cavalieri, D.J., 2008. Arctic sea ice variability and trends, 1979–2006. J. Geophys. Res. 113, C07003–28. doi:10.1029/2007JC004558

Perovich, D.K., 2006. The interaction of ultraviolet light with Arctic sea ice during SHEBA. Annals of glaciology.

Poulain, A.J., Ni Chadhain, S.M., Ariya, P.A., Amyot, M., Garcia, E., Campbell, P.G.C., Zylstra, G.J., Barkay, T., 2007. Potential for Mercury Reduction by Microbes in the High Arctic. Applied and Environmental Microbiology 73, 2230–2238. doi:10.1128/AEM.02701-06

Rutgers van der Loeff, M.M., Cassar, N., Nicolaus, M., Rabe, B., Stimac, I., 2014. The influence of sea ice cover on air-sea gas exchange estimated with radon-222 profiles. J. Geophys. Res.-Oceans 119, 2735-2751. doi: 10.1002/2013JC009321

Sanei, H., Outridge, P.M., Goodarzi, F., Wang, F., Armstrong, D., Warren, K., Fishback, L., 2010. Wet deposition mercury fluxes in the Canadian sub-Arctic and southern Alberta, measured using an automated precipitation collector adapted to cold regions. Atmospheric Environment 44, 1672–1681. doi:10.1016/j.atmosenv.2010.01.030

Schlitzer, R., 2015. Ocean Data View, odv.awi.de.

Schroeder, W.H., Anlauf, K.G., Barrie, L.A., Lu, J.Y., Steffen, A., Schneeberger, D.R., Berg, T., 1998. Arctic springtime depletion of mercury. Nature 394, 331–332. doi:10.1038/28530

Screen, J.A., Simmonds, I., 2010. The central role of diminishing sea ice in recent Arctic temperature amplification. Nature 464, 1334–1337. doi:10.1038/nature09051

Serreze, M.C., Barrett, A.P., Slater, A.G., Woodgate, R.A., Aagaard, K., Lammers, R.B., Steele, M., Moritz, R., Meredith, M., Lee, C.M., 2006. The large-scale freshwater cycle of the Arctic. J. Geophys. Res. 111, 14485–20. doi:10.1029/2005JC003424

Slemr, F., Schuster, G., Seiler, W., 1985. Distribution, speciation, and budget of atmospheric

mercury. J Atmos Chem 3, 407–434. doi:10.1007/BF00053870

Soerensen, A.L., Jacob, D.J., Schartup, A., 2016. A mass budget for mercury and methylmercury in the Arctic Ocean. Global …. doi:10.1002/(ISSN)1944-9224

Soerensen, A.L., Mason, R.P., Balcom, P.H., Jacob, D.J., Zhang, Y., Kuss, J., Sunderland, E.M., 2014. Elemental Mercury Concentrations and Fluxes in the Tropical Atmosphere and Ocean. Environ. Sci. Technol. 48, 11312–11319. doi:10.1021/es503109p

Soerensen, A.L., Mason, R.P., Balcom, P.H., Sunderland, E.M., 2013. Drivers of Surface Ocean Mercury Concentrations and Air–Sea Exchange in the West Atlantic Ocean. Environ. Sci. Technol. 47, 7757–7765. doi:10.1021/es401354q

Soerensen, A.L., Sunderland, E.M., Holmes, C.D., Jacob, D.J., Yantosca, R.M., Skov, H., Christensen, J.H., Strode, S.A., Mason, R.P., 2010. An Improved Global Model for Air-Sea Exchange of Mercury: High Concentrations over the North Atlantic. Environ. Sci. Technol. 44, 8574–8580. doi:10.1021/es102032g

Sommar, J., Wängberg, I., Berg, T., 2007. Circumpolar transport and air-surface exchange of atmospheric mercury at Ny-Ålesund (79° N), Svalbard, spring 2002. Atmospheric ….

Steffen, A., Bottenheim, J., Cole, A., Ebinghaus, R., Lawson, G., Leaitch, W.R., 2014. Atmospheric mercury speciation and mercury in snow over time at Alert, Canada. Atmos. Chem. Phys. 14, 2219–2231. doi:10.5194/acp-14-2219-2014

Steffen, A., Douglas, T., Amyot, M., Ariya, P., Aspmo, K., Berg, T., Bottenheim, J., Brooks, S., Cobbett, F., Dastoor, A., Dommergue, A., Ebinghaus, R., Ferrari, C., Gårdfeldt, K., Goodsite, M.E., Lean, D., Poulain, A.J., Scherz, C., Skov, H., Sommar, J., Temme, C., 2008. A synthesis of atmospheric mercury depletion event chemistry in the atmosphere and snow. Atmos. Chem. Phys. 8, 1445–1482. doi:10.5194/acp-8-1445-2008

Steffen, A., Lehnherr, I., Cole, A., Ariya, P., Dastoor, A., Durnford, D., Kirk, J., Pilote, M., 2015. Atmospheric mercury in the Canadian Arctic. Part I: A review of recent field measurements. Science of the Total Environment, The 509-510, 3–15. doi:10.1016/j.scitotenv.2014.10.109

Stern, G.A., Macdonald, R.W., Outridge, P.M., Wilson, S., Chételat, J., Cole, A., Hintelmann, H., Loseto, L.L., Steffen, A., Wang, F., Zdanowicz, C., 2012. How does climate change influence arctic mercury? Science of the Total Environment, The 414, 22–42. doi:10.1016/j.scitotenv.2011.10.039

Strode, S.A., Jaeglé, L., Selin, N.E., Jacob, D.J., Park, R.J., Yantosca, R.M., Mason, R.P., Slemr, F., 2007. Air-sea exchange in the global mercury cycle. Global Biogeochem. Cycles 21, n/a–n/a. doi:10.1029/2006GB002766

Tschudi, M., C. Fowler, J. Maslanik, J. S. Stewart, and W. Meier. 2016. *EASE-Grid Sea Ice Age*. Boulder, Colorado USA: NASA National Snow and Ice Data Center Distributed Active Archive Center. http://dx.doi.org/10.5067/PFSVFZA9Y85G.

Tseng, C.M., Lamborg, C.H., Hsu, S.C., 2013. A unique seasonal pattern in dissolved elemental mercury in the South China Sea, a tropical and monsoon-dominated marginal sea. Geophys. Res. Lett. 40, 167–172. doi:10.1029/2012GL054457

U.S. Environmental Protection Agency, 2002. Method 1631, Revision E: Mercury in Water by Oxidation, Purge and Trap, and Cold Vapor Atomic Fluorescence Spectrometry. US EPA Office of Science and Technology, Washington, D.C.

Wang, F., Macdonald, R.W., Stern, G.A., Outridge, P.M., 2010. When noise becomes the signal: Chemical contamination of aquatic ecosystems under a changing climate. Marine Pollution Bulletin 60, 1633–1635. doi:10.1016/j.marpolbul.2010.05.018